Tissue-engineered Cardiac Patch for Advanced Functional Maturation of Human ESC-derived Cardiomyocytes

Donghui Zhang[1],PhD, Ilya Shadrin[1],BS, Jason Lam[2],PhD, Hai-Qian Xian[2],PhD, Ralph Snodgrass[2],PhD, and Nenad Bursac[1]*, PhD

[1]Department of Biomedical Engineering, Duke University, Durham, NC
[2]VistaGen Therapeutics, Inc., San Francisco, CA

Short title: Functional human engineered cardiac tissue

*Corresponding author:

Nenad Bursac, PhD
Associate Professor of Biomedical Engineering
Faculty of Cardiology
Duke University
3000 Science Drive
Hudson Hall, Room 136
Durham, NC 27708
phone: 919-660-5510
fax: 919-684-4488
e-mail: nbursac@duke.edu

Abstract

Human embryonic stem cell-derived cardiomyocytes (hESC-CMs) provide a promising source for cell therapy and drug screening. Several high-yield protocols exist for hESC-CM production; however, methods to significantly advance hESC-CM maturation are still lacking. Building on our previous experience with mouse ESC-CMs, we investigated the effects of 3-dimensional (3D) tissue-engineered culture environment and cardiomyocyte purity on structural and functional maturation of hESC-CMs. 2D monolayer and 3D fibrin-based cardiac patch cultures were generated using dissociated cells from differentiated Hes2 embryoid bodies containing varying percentage (48-90%) of CD172a (SIRPA)-positive cardiomyocytes. hESC-CMs within the patch were aligned uniformly by locally controlling the direction of passive tension. Compared to hESC-CMs in age (2 weeks) and purity (48-65%) matched 2D monolayers, hESC-CMs in 3D patches exhibited significantly higher conduction velocities (CVs), longer sarcomeres (2.09±0.02 vs. 1.77±0.01 μm), and enhanced expression of genes involved in cardiac contractile function, including cTnT, αMHC, CASQ2 and SERCA2. The CVs in cardiac patches increased with cardiomyocyte purity, reaching 25.1 cm/s in patches constructed with 90% hESC-CMs. Maximum contractile force amplitudes and active stresses of cardiac patches averaged to 3.0±1.1 mN and 11.8±4.5 mN/mm^2, respectively. Moreover, contractile force per input cardiomyocyte averaged to 5.7±1.1 nN/cell and showed a negative correlation with hESC-CM purity. Finally, patches exhibited significant positive inotropy with isoproterenol administration (1.7±0.3-fold force increase, EC_{50} = 95.1 nM). These results demonstrate highly advanced levels of hESC-CM maturation after 2 weeks of 3D cardiac patch culture and carry important implications for future drug development and cell therapy studies.

Key Words: Human pluripotent stem cells, hydrogel, optical mapping, adrenergic stimulation, cardiac tissue engineering

Introduction

Since the discovery of human embryonic (hESCs) and induced pluripotent stem cells (hiPSCs), significant efforts have been made to enable efficient production of human cardiomyocytes (CMs) [1]. Of particular importance to clinical translation are the recently developed techniques for high-yield cardiac differentiation that do not require the use of genetic modifications [2-7]. Furthermore, new purification protocols based on cell-surface markers (SIRPA, VCAM1) [8, 9], mitochondrial fluorescence dyes (TMRM)[10], or distinct metabolic flows in CMs and non-CMs [11] have enabled generation of virtually pure (>95%) cardiomyocyte populations. Despite these advances, human pluripotent stem cell-derived cardiomyocytes (hPSC-CMs) retain a relatively immature phenotype and, unlike their adult counterparts, exhibit relatively small size, reduced electrical excitability [1, 12], impaired excitation-contraction coupling [13-17] and incomplete adrenergic sensitivity [18, 19]. The lack of robust methodologies to promote functional maturation of human cardiomyocytes is currently one of the critical obstacles to the successful development of predictive drug and toxicology screens as well as safe and efficient cardiac therapies.

In general, functional maturity of cardiomyocytes at the tissue level is evidenced by their ability to support fast action potential conduction and generate high contractile stresses. Previously, genetically purified (>95%) hiPSC-CMs were shown to support relatively fast (~21 cm/s) electrical conduction in 2D cultures (monolayers) [20], although similar velocities have not been achieved in a handful of studies that assessed the functional output of engineered 3D human heart tissues [19, 21-23]. In the best reported case [21], tissues made of genetically purified hESC-CMs exhibited contractile stresses (4.4 mN/mm^2) and conduction velocities (<4.9 cm/s), an order of magnitude lower than adult human myocardium (20-45 mN/mm^2 and 40-50 cm/s) [24, 25]. As such, it remains unknown whether hPSC-CMs can be matured *in vitro* to attain both high CVs and contractile stresses, as well as how cardiomyocyte purity and 3D culture affect functional output and maturation of human engineered cardiac tissues.

To address these questions, we generated 2D and 3D cultures of human ESC-CMs based on our recent experience engineering functional cardiac tissues using mouse ESC-CMs [26]. The goal of 3D culture model was to assess the electrical and mechanical maturation of hESC-CM. Specifically, quantification of electrical impulse propagation and mechanical force generation was used to assess the overall tissue function, with subsequent immunofluorescence and genetic profiling to assess the structural and molecular properties of the hESC-CMs. Finally, levels of advanced maturity were assessed using beta-adrenergic stimulation of the engineered tissues.

Materials and Methods

Cardiac differentiation of hESCs

Human ES cells (HES-2 line) were trypsin-adapted and differentiated to a cardiovascular lineage based on previously described methods (Fig. S1A) [9]. Briefly, two days prior to differentiation (d-2), hESCs were plated on Matrigel (BD Biosciences) coated plates for feeder depletion. EBs were formed by aggregating trypsinized ES cell clusters in StemPro-34 media containing BMP4 (0.5 ng/ml) in low-attachment plates overnight (d-1) in humidified incubator and cultured under hypoxic conditions (5% O_2, 5% CO_2, 37°C) until day 11. On day 0 (start of differentiation), EBs were harvested and resuspended in Induction Medium (StemPro-34, bFGF (5 ng/ml), activin A (6 ng/ml) and BMP4 (10 ng/ml)) and cultured for 3 days. On day 4, EBs were harvested and resuspended in StemPro-34 supplemented with VEGF (10 ng/ml) and Wnt-C59 (2 μM, Cellagen Technology). Medium was exchanged on day 6 with StemPro-34 supplemented with VEGF (10 ng/ml). On day 8, 11, and 15, medium was exchanged with StemPro-34 supplemented with only VEGF (10 ng/ml) and bFGF (5 ng/ml). On day 11, EBs were moved from hypoxic (5% O_2, 5% CO_2, 37°C) to ambient oxygen condition (5% CO_2, ambient air, 37°C). From day 18 on, medium was replaced with fresh 2% FBS/DMEM every 3 days. hESC-CMs were used on days 22-30 of differentiation. All StemPro-34 media included L-glutamine (2 mM), transferrin (150 μg/ml, Roche), ascorbic acid (50 μg/ml), and monothioglycerol (0.45 mM). Medium supplements were purchased from Life Technologies Corporations, unless otherwise stated. Chemicals were obtained from Sigma Aldrich and all growth factors were obtained from R&D Systems.

Dissociation of differentiated cell clusters

Beating cell clusters were dissociated using 0.2% collagenase type I (Sigma C-0130) in 20% FBS/DMEM (Gibco) at 37°C for 1 hour, followed by 0.25% trypsin/EDTA (Cellgro) with gentle shaking in a 37°C water bath for 5-7 minutes. Single-cell suspension was achieved by triturating with equal volume of 50% FBS/DMEM + 20μg/ml DNase (Calbiochem).

Purification of hESC-CMs

For monolayer and patch cultures, the fraction of cardiomyocytes in dissociated cells was enriched by magnetic-activated cell sorting (MACS). Briefly, dissociated cells ($5x10^6$ cells/ml) were stained with PE-Cy7 conjugated anti-SIRPA-IgG antibody (clone SE5A5; BioLegend; 1:500). Labeled cells were loaded with anti-PE-Cy7 MicroBeads, and the cell/bead mix was passed through MS Columns on a MiniMACS™ separator (Miltenyi Biotec). Small fractions of immunolabeled cells (MSC sorted and unsorted) were then analyzed using the flow cytometer FACSAria II with FACSDiva software, version 6.0 (BD Biosciences). Cardiac specificity of SIRPA was confirmed by FACS analysis (Fig. S1B-D) for cardiac troponin T (cTnT) which showed that >92% of $SIRPA^+$ cells in MACS sorted and unsorted populations consisted of $cTnT^+$ cardiomyocytes. Based on this analysis, MACS sorted and unsorted cells were mixed in different ratios to obtain 48-90% pure hESC-CM populations used for patch and monolayer production.

Cardiac patch fabrication and culture

To generate aligned 3D human cardiac tissue patches, $7x7mm^2$ polydimethylsiloxane (PDMS, Dow Corning) molds with staggered hexagonal posts (1.2 mm long) were microfabricated as previously described [27]. Hydrogel solution (24 μL fibrinogen (10 mg/mL), 12 μL Matrigel, 24 μL 2x cardiac media)) was mixed with $1x10^6$ cells in 59 μL cardiac media to obtain a total of 120 μl of cell/gel solution. Following addition of thrombin (0.92 μL), cell/gel solution was added to PDMS molds containing a Velcro frame and left at 37ºC for 1hr to polymerize. Resulting cardiac patches were cultured with rocking in cardiac medium (5% FBS/DMEM with 1mM sodium pyruvate (Gibco), 2mM Glutamine (Gibco), 0.1mM non-essential amino acids (Gibco), 50 μg/ml Ascorbic Acid (Sigma), and 0.45mM monothioglycerol (Sigma)) for 4-14 days. Culture media was supplemented daily with 1mg/mL aminocaproic acid (Sigma) to prevent fibrin degradation. 10μM BrdU (Sigma) was added on day 0 of patch culture to inhibit proliferation of non-myocytes and preserve initial purity of hESC-CMs. BrdU was removed after 24 h of culture, and media was changed every 2 days thereafter.

Assessment of electrical propagation

Optical mapping of transmembrane potentials was performed after 2 weeks of culture using our established methods [26, 28, 29]. Two-second episodes of electrical activity induced by stimulation with point electrode were recorded in macroscopic (whole tissue) or microscopic (4x objective on a Nikon microscope) mode using a 504-channel photodiode array (RedShirt Imaging) or a fast EMCCD camera ($iXon^{EM}+$, Andor). Data analysis was performed using custom MATLAB software [28].

Assessment of contractile force generation

Force generating capacity of cardiac tissue patches was assessed in 2-week old patches loaded into a custom-made isometric force measurement setup containing a sensitive optical force transducer and a computer-controlled linear actuator (Thorlabs), as previously described [26, 29, 30]. Inotropic responsiveness of the tissue patches was tested by measurement of contractile force generation in the presence of 10^{-10}, 10^{-9}, 10^{-8}, 10^{-7}, 10^{-6} and 10^{-5} M β-adrenergic agonist isoproterenol in 0.9mM Ca^{2+} Tyrode's solution during 1Hz electrical stimulation at 10% stretch.

Statistical analysis

Experimental data reported as mean ± SEM was compared by one-way ANOVA and unpaired t-test. Wilcoxon Rank-Sum test (median, Z-score, p-value) was used for non-normal distributions. A bivariate linear regression analysis was performed to determine significance of linear fits. A p-value of 0.05 was considered significant.

Additional details and assessment methodologies are provided in Supplemental Materials.

Results

Electrophysiological properties of hESC-CMs

Action potential properties of dissociated unpurified hESC-CMs were assessed using patch-clamp recordings. After 20-30 days of differentiation cardiomyocytes exhibited a predominantly ventricular action potential (AP) phenotype with hyperpolarized resting membrane potentials (-70.9±0.5 mV) and relatively fast maximum upstroke velocities (38.1±1.5 V/s) (Fig. S2A). Studied hESC-CMs exhibited expected dose-dependent responses to HERG K^+ channel blocker E-4031, L-type Ca^{2+} channel blocker nifedipine, and ATP-sensitive K^+ channel blocker terfenadine (Fig. S2B). Specifically, the application of E-4031 and terfenadine caused a significant increase in action potential duration at 90% repolarization (APD90), while nifedipine caused a large decrease in APD90 (Fig. S2C), showing physiological responses to inhibition of K^+ and Ca^{2+} channels.

Structural phenotype of human cardiac tissue patches and monolayers

Differentiated cell populations with varying hESC-CM purity (48-90%) were cultured in 20 mm-diameter confluent monolayers and 7x7mm^2 porous 3D cardiac tissue patches (Fig. 1A-B, Movie 1). Elliptical pores in the patches facilitated nutrient transport and enabled the formation of uniformly dense and aligned cardiac tissue [26] (Fig. 1C and S3). Immunostaining for cardiac markers revealed aligned cardiomyocytes that exhibited cross-striated patterns of troponin T (cTnT, Fig. 1D), myosin heavy chain (MHC, Fig. 1E) and α-actinin (SAA, Fig. 2A), indicative of well-developed sarcomeric structures. Additionally, N-cadherin and connexin-43 (Cx43) immunostaining demonstrated presence of intercellular gap and adherens junctions, respectively, suggestive of functional electromechanical coupling between cardiomyocytes (Fig. 1F and 2A). Confocal analysis of non-cardiac cell markers revealed the presence of $SM22\alpha^+$ smooth muscle cells (Fig. 1F) that resided primarily at the patch surface along with vWF^-/Vim^+ fibroblasts (Fig. S4), while vWF^+/Vim^+ endothelial cells (Fig. 1F) occupied the patch interior (Fig. S4). Similar to 3D patches, 2D monolayer cultures

also contained cross-striated hESC-CMs (Fig. 2B) interspersed with both fibroblasts and vascular cells (data not shown). Importantly, hESC-CMs in 3D tissue patches exhibited significantly longer sarcomeres then in 2D monolayers (2.09±0.02 vs. 1.77±0.01 μm, Fig. 2C,D), reaching optimal sarcomere length measured in adult human cardiomyocytes [31].

Time course of cardiac gene expression

Using qRT-PCR, we assessed expression of pluripotency and cardiac-specific genes (for the list of primers see Table S1) in undifferentiated hESCs, differentiated hESCs, and cardiac patches and monolayers at different times of culture. As expected, OCT4 and NANOG expression decreased significantly during hESC differentiation and virtually disappeared in patches (Fig. 3A,B) and monolayers (not shown). Early cardiac markers ISL1 and GATA4 increased with cardiac differentiation, with ISL1 decreasing during subsequent patch culture (Fig. 3C). Consistent with human ventricular development [32, 33], gene expression levels of βMHC and MLC2v increased and αMHC decreased during patch culture, yielding a significant increase in βMHC/αMHC and MLC2v/MLC2a expression ratios (Fig. 3D-F). Furthermore, expression of genes that determine AP shape and propagation (Fig. 3G) either increased with tissue patch culture (Cx43, $Na_v1.5$, $K_v4.3$) or remained unchanged (Kir2.1, $Ca_v1.2$). Interestingly, genes crucial for excitation-contraction (E-C) coupling (CASQ2, SERCA2) were significantly upregulated during 2-week patch culture (Fig. 3H,I), showing a 170-fold increase in calsequestrin expression that was previously shown to be lacking in 2D cultured hESC-CMs [13, 14]. Compared to 2D monolayers, hESC-CMs in 3D patches had significantly upregulated genes required for cardiac E-C coupling (Fig. 3H,I) and contractile function (cTnT, αMHC, Fig. S5). In contrast, culture environment (2D vs. 3D) had no major influence on genes important for cardiac electrical function (Fig. 3G).

Action potential conduction in cardiac patches and monolayers

Optical mapping of transmembrane potentials (Fig. 4A) revealed macroscopically continuous action potential propagation in both tissue patches (Fig. 4B, Movie 2) and monolayers (Fig. 4C, Movie 3). Interestingly, conduction velocity (CV) in cardiac patches increased linearly with hESC-CM purity, reaching 25.1 cm/s in patches made of 90% cardiomyocytes (Fig. 4D). Compared to age- and purity- (48-65%) matched 2D monolayers, 3D patches exhibited significantly higher CVs (9.76±1.0 vs. 5.17±0.7 cm/s, Fig. 4D), but not significantly different action potential durations (APD, 338±30 vs. 278±20 ms, Fig. 4E) or maximum capture rates (MCR, 2.6±0.2 vs. 2.6±0.1 Hz, Fig. 4F). In contrast to CVs, neither APDs nor MCRs in patches or monolayers showed significant correlation with hESC-CM purity. Both CV and APD in patches decreased with increased pacing frequency (electrical restitution), while monolayers showed only significant APD restitution (Fig. S6A,B). Thus, 3D cardiac patches appeared to form a more functional electrical syncytium than 2D monolayers.

Contractile properties of cardiac tissue patches

Assessment of isometric force generation revealed that electrically stimulated cardiac tissue patches generated active forces (twitch contractions) that increased with applied stretch in a Frank-Starling-like fashion (Fig. 5A,B). Maximum active (contractile) forces averaged to 3.0±1.1 mN and showed no significant correlation with hESC-CM purity (Fig. 5C). Based on

measurements of the patch width (7 mm), thickness (73.6±6.6 μm, Fig. S3), percent pore area in the patch (porosity, 39.5±4.9%), and distribution of cell alignments [30], we estimated the average contractile stress in our cardiac patches to be 11.8±4.5 mN/mm^2. Since methods to calculate contractile stress amplitudes may vary among different research groups, we also calculated a functional parameter that can serve to quantify the "efficiency of a cardiac tissue engineering system" by dividing the contractile force amplitude in each cardiac patch (system output) with the number of cardiomyocytes used to make the patch (system input). The calculated contractile-force-per-input-cardiomyocyte in our patches averaged to 5.7±1.0 nN/cell and decreased with increase in hESC-CM purity (Fig. 5D). Similar to active forces, passive tension in patches increased with applied stretch (Fig. 5B), but significantly decreased with hESC-CM purity (Fig. S7A), yielding a linear increase in the active:passive force ratio for patches with higher hESC-CM purity (Fig. S7B). Along with being mechanically softer, patches made with higher percent cardiomyocytes also displayed shorter twitch rise times (Fig. S7C,D).

Finally, we tested the sensitivity of engineered cardiac tissue patches to beta-adrenergic stimulation. Increasing doses of β-adrenergic agonist isoproterenol caused an expected increase in spontaneous contraction frequency (data not shown) as well as a sigmoidal increase in twitch amplitude (up to ~1.7±0.3 fold with EC_{50} of 95.1 nM, Fig. 6A,B). Furthermore, increasing isoproterenol concentrations yielded significant shortening of twitch rise time (Fig. 6C) indicative of accelerated force generation. Together with the results of structural, gene expression, and electrophysiological analyses, the high contractile stresses and inotropic responsiveness to adrenergic stimulation collectively demonstrated advanced functional maturation of hESC-CMs in the cardiac tissue patches.

Discussion

In this study, we generated relatively large, aligned, and highly functional cardiac tissue patches using human embryonic stem cell-derived cardiomyocytes. Our results demonstrate that after only two weeks of culture, the optimized 3D environment of a cardiac tissue patch can yield advanced levels of structural and functional maturation of hESC-CMs, as evidenced by their mature sarcomeric organization, enhanced cardiac gene expression profiles, and robust functional output. Specifically, we show that: 1) aligned human heart tissues can be engineered with a sheet-like (rather than cable) geometry and exhibit both high CVs (up to 25.1 cm/s) and contractile forces and stresses (3.0 mN and 11.8 mN/mm^2), 2) initial hESC-CM purity uniquely determines the electromechanical properties of the engineered myocardium, and 3) hESC-CM maturation in optimized 3D patch environment is enhanced relative to that in standard 2D cultures. Additionally, engineered cardiac tissue patches demonstrated significant adrenergic responsiveness, confirming the advanced maturation state of hESC-CMs. These results build on our previous studies that established the optimal *in vitro* conditions for the formation of mouse ESC-derived myocardium and demonstrated a requisite role of non-cardiomyocytes in this process [26]. Similarly, in this study, the formation and/or maturation of functional human myocardium may have been supported by the presence of endothelial, smooth muscle, and fibroblastic cells in the patch. These cells have been differentiated together with cardiomyocytes from the same hESC

source, thus avoiding the need for supplementation with exogenous non-cardiac cells, as employed in previous studies [21, 23, 34].

Methods for engineering contractile human cardiac tissues from pluripotent stem cell-derived cardiomyocytes have involved the use of scaffold-free cell sheets [35], porous polymer scaffolds [34], and different hydrogels, including collagen [21-23, 36], fibrin [19], and cardiac ECM-derived hydrogels [37]. Among these studies, only four [19, 21-23] have assessed tissue contractile function and only one [21] has also assessed electrical function of the engineered myocardium. Compared to these reports, cardiac tissue patches generated in our study exhibit 2.2-180-fold and 2.6-150-fold higher contractile force and stress generation, respectively (see Table S2 for all previous reports on functional assessment of primary and stem cell-derived engineered cardiac tissues). Due to a lack of standardized methods to calculate contractile stress amplitude (e.g. in geometrically complex tissues), we also introduced a unifying metric for quantifying the efficiency of a cardiac tissue engineering approach by dividing the maximum contractile force of a cardiac construct by the number of cardiomyocytes used for its production. Using this metric, we further showed 4-700-fold higher efficiency of our cardiac tissue approach (average force-per-CM ratio of 5.7 nN/cell) than previously achieved (Fig. 5D, Table S2). In addition, the maximum velocities of action potential propagation achieved in this study (at 80-90% hESC-CM purity) represent a 5-fold increase compared to previous reports in human engineered tissues [21] (Table S2). Overall, cardiac tissue patches exhibited high contractile stresses and conduction velocities that are only 2-3 times lower than those reported for adult human myocardium (Table S2).

We also explored the effects of the initial hESC-CM purity on electromechanical properties of the engineered cardiac tissues. We found that higher CM purities produced faster CVs but had no significant effect on contractile force production (at least for 48-90% purity), thus yielding a decrease in force-per-input-cardiomyocyte ratio. While higher CM purity (i.e. less non-myocytes) would expectedly facilitate cardiomyocyte contacts and increase CV, lack of force augmentation may result from a limit on the CM survival in a given patch volume. Thus, the use of hydrogels seeded at low density with high purity of hESC-CMs may be the most efficient strategy to maximize CM survival and electromechanical output of 3D engineered myocardium. This strategy could be used for the optimal design of high-throughput screening platforms that employ 3D functional engineered cardiac tissues while utilizing minimum numbers of human CMs.

Furthermore, we demonstrated that relative to standard 2D culture, 3D patch environment significantly enhanced hESC-CM maturation. Specifically, on a structural level, 3D culture promoted an increase in sarcomere length to values comparable to those of adult human cardiomyocytes. Previously, sarcomere lengthening in hiPSC- and hESC-CMs was induced through mechanical stretch [21]; however, achieved sarcomere lengths remained at sub-adult values [31]. Interestingly, the 3D patch culture also enhanced expression of genes determining cardiac contractile function and Ca^{2+} handling (cTnT, αMHC, SERCA2, CASQ2) but not electrical function (Cx43, $Na_v1.5$, Kir2.1, $Ca_v1.2$). Combined with studies showing high CVs in relatively pure hiPSC-CM monolayers [20], our results suggest that 2D monolayers and 3D sheet-like patches may be of similar utility for studies of cardiac impulse propagation and related arrhythmogenesis. On the other hand, the advanced structural and contractile characteristics of hESC-CMs in 3D cardiac patches would render them preferred

over 2D monolayers for physiological and pharmacological studies of cardiac contractile function and excitation-contraction coupling.

In support of this notion, cardiac patches were found to exhibit a robust inotropic response (i.e. an increased amplitude and faster kinetics of force generation) to a β-adrenergic agonist, isoproterenol. The inotropic effects of isoproterenol are characteristic of the adult human myocardium and require a functional sarcoplasmic reticulum, capable of releasing larger amounts of Ca^{2+} more quickly upon adrenergic stimulation [38, 39]. While this effect has been previously observed in some hESC-CM preparations [21, 40] but not others [18, 19], the relative sensitivity of the inotropic response to isoproterenol was not assessed. Our measured EC_{50} of 95.1 nM falls in the 30-160 nM range reported for adult human ventricular tissue [41, 42], suggesting a near-physiological sensitivity to adrenergic stimulation.

Conclusion

We have established methodologies for successful engineering of a highly functional human cardiac tissue patch starting from hESC-derived cardiomyocytes. The structural and functional properties of these 3D tissue patches, along with the resultant maturation state of hESC-CMs, surpass all previous reports for engineered human myocardium and currently provide the closest *in vitro* approximation of native human heart tissue. Overall, the use of non-genetic methods to purify human pluripotent stem cell-derived CMs, the derivation of vascular cells along with cardiomyocytes, aligned tissue structure, and robust functional output of the obtained cardiac patches all warrant the future use of this tissue-engineering platform for predictive drug and toxicology testing and development of effective cell-based cardiac therapies.

Acknowledgements

The authors thank B. Liau and C. Jackman for technical assistance with patch culture, and R. Kirkton for assistance with optical mapping. This project was supported in part by NIH-NHLBI grants R01HL104326 and R21HL095069 to N.B.

References

[1] Mummery CL, Zhang J, Ng ES, Elliott DA, Elefanty AG, Kamp TJ. Differentiation of human embryonic stem cells and induced pluripotent stem cells to cardiomyocytes: a methods overview. Circ Res. 2012;111:344-58.

[2] Lian X, Zhang J, Azarin SM, Zhu K, Hazeltine LB, Bao X, et al. Directed cardiomyocyte differentiation from human pluripotent stem cells by modulating Wnt/beta-catenin signaling under fully defined conditions. Nat Protoc. 2012;8:162-75.

[3] Minami I, Yamada K, Otsuji TG, Yamamoto T, Shen Y, Otsuka S, et al. A small molecule that promotes cardiac differentiation of human pluripotent stem cells under defined, cytokine- and xeno-free conditions. Cell Rep. 2012;2:1448-60.

[4] Mummery CL, Ward D, Passier R. Differentiation of human embryonic stem cells to cardiomyocytes by coculture with endoderm in serum-free medium. Curr Protoc Stem Cell Biol. 2007;Chapter 1:Unit 1F 2.

[5] Zhang J, Klos M, Wilson GF, Herman AM, Lian X, Raval KK, et al. Extracellular matrix promotes highly efficient cardiac differentiation of human pluripotent stem cells: the matrix sandwich method. Circ Res. 2012;111:1125-36.
[6] Lian X, Hsiao C, Wilson G, Zhu K, Hazeltine LB, Azarin SM, et al. Robust cardiomyocyte differentiation from human pluripotent stem cells via temporal modulation of canonical Wnt signaling. Proceedings of the National Academy of Sciences of the United States of America. 2012;109:E1848-57.
[7] Kattman SJ, Witty AD, Gagliardi M, Dubois NC, Niapour M, Hotta A, et al. Stage-specific optimization of activin/nodal and BMP signaling promotes cardiac differentiation of mouse and human pluripotent stem cell lines. Cell Stem Cell. 2011;8:228-40.
[8] Elliott DA, Braam SR, Koutsis K, Ng ES, Jenny R, Lagerqvist EL, et al. NKX2-5(eGFP/w) hESCs for isolation of human cardiac progenitors and cardiomyocytes. Nature methods. 2011;8:1037-40.
[9] Dubois NC, Craft AM, Sharma P, Elliott DA, Stanley EG, Elefanty AG, et al. SIRPA is a specific cell-surface marker for isolating cardiomyocytes derived from human pluripotent stem cells. Nat Biotechnol. 2011;29:1011-8.
[10] Hattori F, Chen H, Yamashita H, Tohyama S, Satoh YS, Yuasa S, et al. Nongenetic method for purifying stem cell-derived cardiomyocytes. Nat Methods. 2010;7:61-6.
[11] Tohyama S, Hattori F, Sano M, Hishiki T, Nagahata Y, Matsuura T, et al. Distinct metabolic flow enables large-scale purification of mouse and human pluripotent stem cell-derived cardiomyocytes. Cell Stem Cell. 2012.
[12] O'Hara T, Virag L, Varro A, Rudy Y. Simulation of the undiseased human cardiac ventricular action potential: model formulation and experimental validation. PLoS Comput Biol. 2011;7:e1002061.
[13] Poon E, Kong CW, Li RA. Human pluripotent stem cell-based approaches for myocardial repair: from the electrophysiological perspective. Molecular pharmaceutics. 2011;8:1495-504.
[14] Binah O, Dolnikov K, Sadan O, Shilkrut M, Zeevi-Levin N, Amit M, et al. Functional and developmental properties of human embryonic stem cells-derived cardiomyocytes. J Electrocardiol. 2007;40:S192-6.
[15] Liu J, Fu JD, Siu CW, Li RA. Functional sarcoplasmic reticulum for calcium handling of human embryonic stem cell-derived cardiomyocytes: insights for driven maturation. Stem Cells. 2007;25:3038-44.
[16] Itzhaki I, Rapoport S, Huber I, Mizrahi I, Zwi-Dantsis L, Arbel G, et al. Calcium handling in human induced pluripotent stem cell derived cardiomyocytes. PLoS One. 2011;6:e18037.
[17] Itzhaki I, Schiller J, Beyar R, Satin J, Gepstein L. Calcium handling in embryonic stem cell-derived cardiac myocytes: of mice and men. Ann N Y Acad Sci. 2006;1080:207-15.
[18] Pillekamp F, Haustein M, Khalil M, Emmelheinz M, Nazzal R, Adelmann R, et al. Contractile properties of early human embryonic stem cell-derived cardiomyocytes: beta-adrenergic stimulation induces positive chronotropy and lusitropy but not inotropy. Stem Cells Dev. 2012;21:2111-21.
[19] Schaaf S, Shibamiya A, Mewe M, Eder A, Stohr A, Hirt MN, et al. Human engineered heart tissue as a versatile tool in basic research and preclinical toxicology. PloS one. 2011;6:e26397.

[20] Lee P, Klos M, Bollensdorff C, Hou L, Ewart P, Kamp TJ, et al. Simultaneous voltage and calcium mapping of genetically purified human induced pluripotent stem cell-derived cardiac myocyte monolayers. Circ Res. 2012;110:1556-63.
[21] Kensah G, Roa Lara A, Dahlmann J, Zweigerdt R, Schwanke K, Hegermann J, et al. Murine and human pluripotent stem cell-derived cardiac bodies form contractile myocardial tissue in vitro. Eur Heart J. 2012: http://dx.doi.org/10.1093/eurheartj/ehs349 [Epub ahead of print].
[22] Streckfuss-Bomeke K, Wolf F, Azizian A, Stauske M, Tiburcy M, Wagner S, et al. Comparative study of human-induced pluripotent stem cells derived from bone marrow cells, hair keratinocytes, and skin fibroblasts. Eur Heart J. 2012: http://dx.doi.org/10.1093/eurheartj/ehs203 [Epub ahead of print].
[23] Tulloch NL, Muskheli V, Razumova MV, Korte FS, Regnier M, Hauch KD, et al. Growth of engineered human myocardium with mechanical loading and vascular coculture. Circ Res. 2011;109:47-59.
[24] Mulieri LA, Hasenfuss G, Leavitt B, Allen PD, Alpert NR. Altered myocardial force-frequency relation in human heart failure. Circulation. 1992;85:1743-50.
[25] Valderrabano M. Influence of anisotropic conduction properties in the propagation of the cardiac action potential. Prog Biophys Mol Biol. 2007;94:144-68.
[26] Liau B, Christoforou N, Leong KW, Bursac N. Pluripotent stem cell-derived cardiac tissue patch with advanced structure and function. Biomaterials. 2011;32:9180-7.
[27] Bian W, Liau B, Badie N, Bursac N. Mesoscopic hydrogel molding to control the 3D geometry of bioartificial muscle tissues. Nature protocols. 2009;4:1522-34.
[28] Pedrotty DM, Klinger RY, Kirkton RD, Bursac N. Cardiac fibroblast paracrine factors alter impulse conduction and ion channel expression of neonatal rat cardiomyocytes. Cardiovascular research. 2009;83:688-97.
[29] Hinds S, Bian W, Dennis RG, Bursac N. The role of extracellular matrix composition in structure and function of bioengineered skeletal muscle. Biomaterials. 2011;32:3575-83.
[30] Bian W, Juhas M, Pfeiler TW, Bursac N. Local tissue geometry determines contractile force generation of engineered muscle networks. Tissue Eng Part A. 2012;18:957-67.
[31] Rubin R, Strayer DS, Rubin E. Rubin's pathology : clinicopathologic foundations of medicine. Sixth Edition. ed. Philadelphia: Wolters Kluwer Health/Lippincott Williams & Wilkins; 2012.
[32] Reiser PJ, Portman MA, Ning XH, Schomisch Moravec C. Human cardiac myosin heavy chain isoforms in fetal and failing adult atria and ventricles. Am J Physiol Heart Circ Physiol. 2001;280:H1814-20.
[33] Lompre AM, Nadal-Ginard B, Mahdavi V. Expression of the cardiac ventricular alpha- and beta-myosin heavy chain genes is developmentally and hormonally regulated. J Biol Chem. 1984;259:6437-46.
[34] Caspi O, Lesman A, Basevitch Y, Gepstein A, Arbel G, Habib IHM, et al. Tissue engineering of vascularized cardiac muscle from human embryonic stem cells. Circ Res. 2007;100:263-72.
[35] Stevens KR, Kreutziger KL, Dupras SK, Korte FS, Regnier M, Muskheli V, et al. Physiological function and transplantation of scaffold-free and vascularized human cardiac muscle tissue. Proc Natl Acad Sci U S A. 2009;106:16568-73.

[36] Duan Y, Liu Z, O'Neill J, Wan LQ, Freytes DO, Vunjak-Novakovic G. Hybrid gel composed of native heart matrix and collagen induces cardiac differentiation of human embryonic stem cells without supplemental growth factors. J Cardiovasc Transl Res. 2011;4:605-15.
[37] Habib M, Shapira-Schweitzer K, Caspi O, Gepstein A, Arbel G, Aronson D, et al. A combined cell therapy and in-situ tissue-engineering approach for myocardial repair. Biomaterials. 2011;32:7514-23.
[38] Brandenburger M, Wenzel J, Bogdan R, Richardt D, Nguemo F, Reppel M, et al. Organotypic slice culture from human adult ventricular myocardium. Cardiovasc Res. 2012;93:50-9.
[39] Dolnikov K, Shilkrut M, Zeevi-Levin N, Gerecht-Nir S, Amit M, Danon A, et al. Functional properties of human embryonic stem cell-derived cardiomyocytes: intracellular Ca2+ handling and the role of sarcoplasmic reticulum in the contraction. Stem Cells. 2006;24:236-45.
[40] He JQ, Ma Y, Lee Y, Thomson JA, Kamp TJ. Human embryonic stem cells develop into multiple types of cardiac myocytes: action potential characterization. Circ Res. 2003;93:32-9.
[41] Flesch M, Schwinger RH, Schiffer F, Frank K, Sudkamp M, Kuhn-Regnier F, et al. Evidence for functional relevance of an enhanced expression of the Na(+)-Ca2+ exchanger in failing human myocardium. Circulation. 1996;94:992-1002.
[42] Holubarsch C, Schneider R, Pieske B, Ruf T, Hasenfuss G, Fraedrich G, et al. Positive and negative inotropic effects of DL-sotalol and D-sotalol in failing and nonfailing human myocardium under physiological experimental conditions. Circulation. 1995;92:2904-10.

Figure legends

Figure 1. Structural properties of human cardiac tissue patches. A) Representative 2-week old cardiac tissue patch anchored within a Velcro frame. B-C) Staggered elliptical pores within the patch (B) are surrounded by densely packed and aligned cells (C). D) hESC-CMs in 2-week old cardiac tissue patches are aligned and show cross-striated patterning of cardiac Troponin T (cTnT). Fibroblasts positive for vimentin (Vim) are interspersed among hESC-CMs. E) hESC-CMs also exhibit cross-striated pattern of myosin heavy chain (MHC) and sarcomeric α-actinin (SAA). F) Cardiac patches show evidence of mechanical coupling (N-cadherin) between hESC-CMs as well as presence of smooth muscle cells (SM22α). Data shown for patches made with 70% hESC-CMs.

Figure 2. hESC-CMs in 3D patches exhibit longer sarcomeres than in 2D monolayers. A) Representative immunostainings of hESC-CMs in 2-week old tissue patch coupled by connexin-43 gap junctions. B) hESC-CMs in 2-week old monolayers. C) Histogram distribution of sarcomere lengths in 2-week old patches and monolayers made with 48-65% hESC-CMs. Note increased sarcomere length in patches vs. monolayers. D) Median and quartile sarcomere lengths in monolayers (n=58 hESC-CMs) and patches (n=106 hESC-CMs). *$p<0.0001$.

Figure 3. Quantitative gene expression during patch and monolayer culture. A-C) qPCR readout of pluripotency (OCT4 and NANOG) and cardiac progenitor (ISL1 and GATA4) genes in undifferentiated hESCs (ES), beating cell clusters (PM0), and cardiac patches at 4 days (P4D), 1 week (P1W), and 2 weeks (P2W) of culture. D-F) qPCR readout of contractile function genes: MHC, myosin heavy chain; cTnT, cardiac Troponin T; MLC2v/a, Myosin light chain 2 ventricular/atrial. G-I) qPCR readout of electrical function (Nav1.5, fast Na^+ channel; Kir2.1, inward rectifier K^+ channel; Kv4.3, transient outward K^+ channel; Cav1.2, L-type Ca^{2+} channel) and excitation-contraction (SERCA2, SR Ca^{2+}-ATPase; CASQ2, calsequestrin) genes in patches and monolayers of the same age (M1W and M2W, 1 and 2 week monolayer) and hESC-CM purity (60-65%). All data except F are shown relative to PM0 group. n = 2–4 biological x 3 technical replicates. $p<0.05$ from: *, PM0; **, all other groups; †, ES; #, another group.

Figure 4. Action potential propagation in cardiac patches and monolayers. A) Representative optically mapped action potential traces in a 2-week old cardiac patch at various pacing rates. B,C) Representative isochrone maps during 1 Hz point stimulation of a 2-week old cardiac patch (B) and monolayer (C). D-F) Conduction velocity (D), action potential duration (E), and maximum capture rate (F) during point stimulation of cardiac patches and monolayers as a function of hESC-CM purity. †$p<0.05$ between patches and monolayers ($48\% <$ hESC-CM purity $< 65\%$.)

Figure 5. Contractile properties of cardiac tissue patches. A) Representative active (contractile) force traces during progressive stretch of an electrically stimulated (1Hz) 2-week cardiac patch. B) Corresponding active and passive force-length relationships in cardiac patches made with 57%-65% hESC-CMs (n=5). C) Maximum contractile force (at 1 Hz

stimulation) in 2-week patches as a function of hESC-CM purity. D) Contractile force per input hESC-CM as a function of cardiomyocyte purity; $p<0.03$ for linear trend.

Figure 6. Inotropic response of cardiac tissue patches to beta-adrenergic stimulation. A) Representative active force traces in a tissue patch made with 55% hESC-CMs during application of increasing doses of isoproterenol (measured at 10% stretch, 1 Hz stimulation, and 0.9 mM extracellular [Ca^{2+}]). B-C) Contractile force amplitude (B) and twitch kinetics (C) as a function of isoproterenol concentration (n=4).

Fig 1.

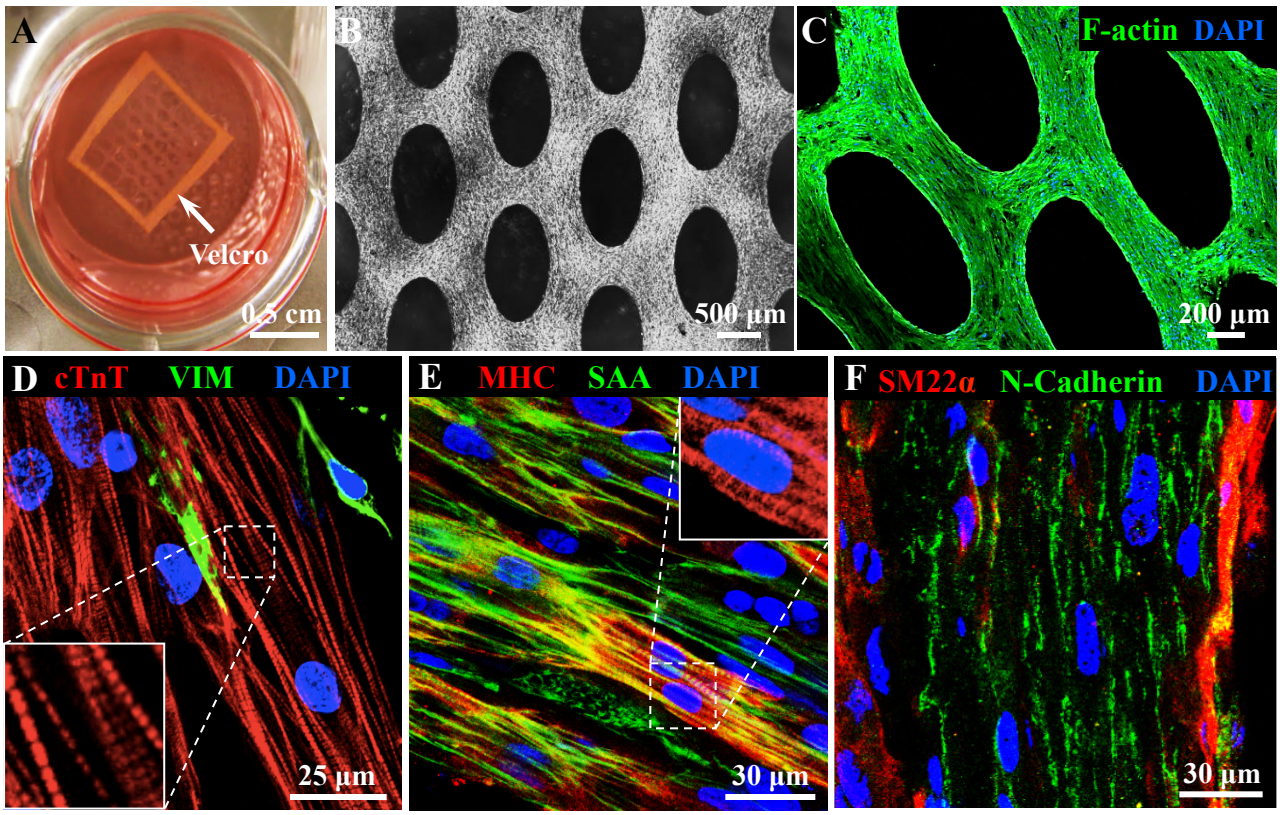

Figure 1. Structural properties of human cardiac tissue patches. A) Representative 2-week old cardiac tissue patch anchored within a Velcro frame. B-C) Staggered elliptical pores within the patch (B) are surrounded by densely packed and aligned cells (C). D) hESC-CMs in 2-week old cardiac tissue patches are aligned and show cross-striated patterning of cardiac Troponin T (cTnT). Fibroblasts positive for vimentin (Vim) are interspersed among hESC-CMs. E) hESC-CMs also exhibit cross-striated pattern of myosin heavy chain (MHC) and sarcomeric α-actinin (SAA). F) Cardiac patches show evidence of mechanical coupling (N-cadherin) between hESC-CMs as well as presence of smooth muscle cells (SM22α). Data shown for patches made with 70% hESC-CMs.

Fig 2.

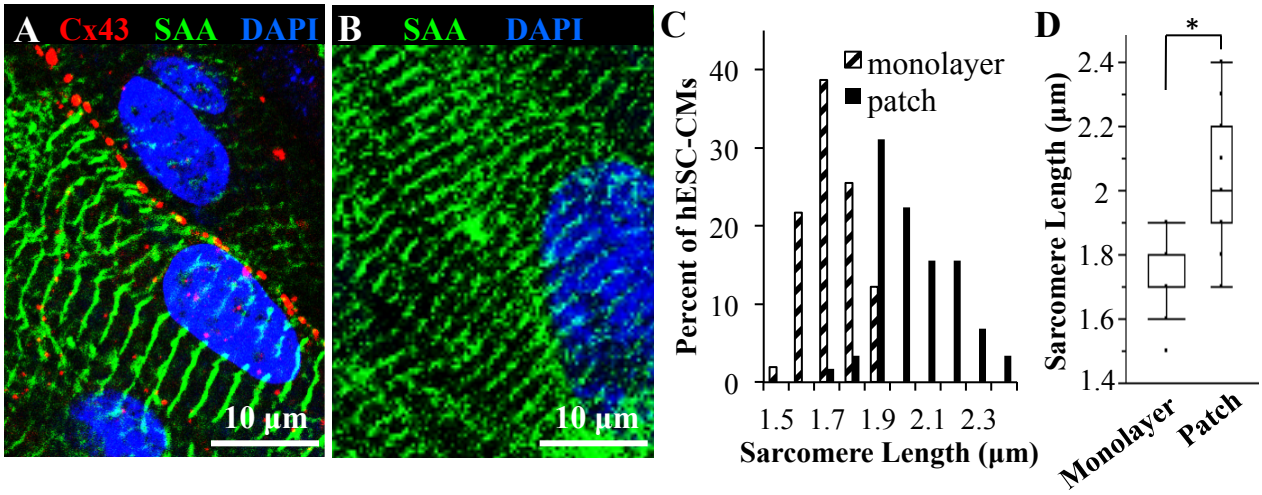

Figure 2. hESC-CMs in 3D patches exhibit longer sarcomeres than in 2D monolayers. A) Representative immunostainings of hESC-CMs in 2-week old tissue patch coupled by connexin-43 gap junctions. B) hESC-CMs in 2-week old monolayers. C) Histogram distribution of sarcomere lengths in 2-week old patches and monolayers made with 48-65% hESC-CMs. Note increased sarcomere length in patches vs. monolayers. D) Median and quartile sarcomere lengths in monolayers (n=58 hESC-CMs) and patches (n=106 hESC-CMs). *$p<0.0001$.

Fig 3.

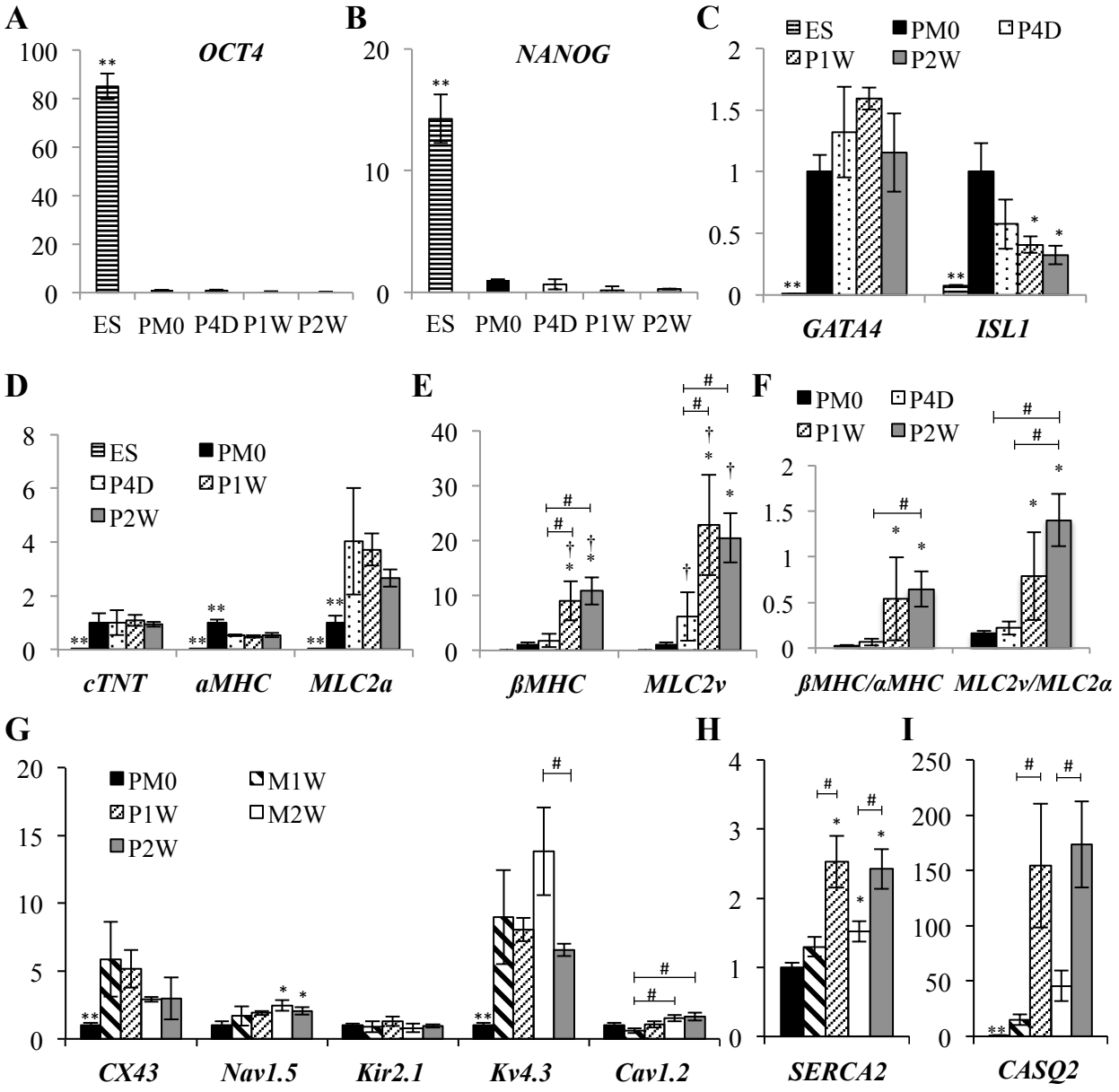

Figure 3. Quantitative gene expression during patch and monolayer culture. A-C) qPCR readout of pluripotency (OCT4 and NANOG) and cardiac progenitor (ISL1 and GATA4) genes in undifferentiated hESCs (ES), beating cell clusters (PM0), and cardiac patches at 4 days (P4D), 1 week (P1W), and 2 weeks (P2W) of culture. D-F) qPCR readout of contractile function genes: MHC, myosin heavy chain; cTnT, cardiac Troponin T; MLC2v/a, Myosin light chain 2 ventricular/atrial. G-I) qPCR readout of electrical function (Nav1.5, fast Na^+ channel; Kir2.1, inward rectifier K^+ channel; Kv4.3, transient outward K^+ channel; Cav1.2, L-type Ca^{2+} channel) and excitation-contraction (SERCA2, SR Ca^{2+}-ATPase; CASQ2, calsequestrin) genes in patches and monolayers of the same age (M1W and M2W, 1 and 2 week monolayer) and hESC-CM purity (60-65%). All data except F are shown relative to PM0 group. n = 2–4 biological x 3 technical replicates. $p<0.05$ from: *, PM0; **, all other groups; †, ES; #, another group.

Fig 4.

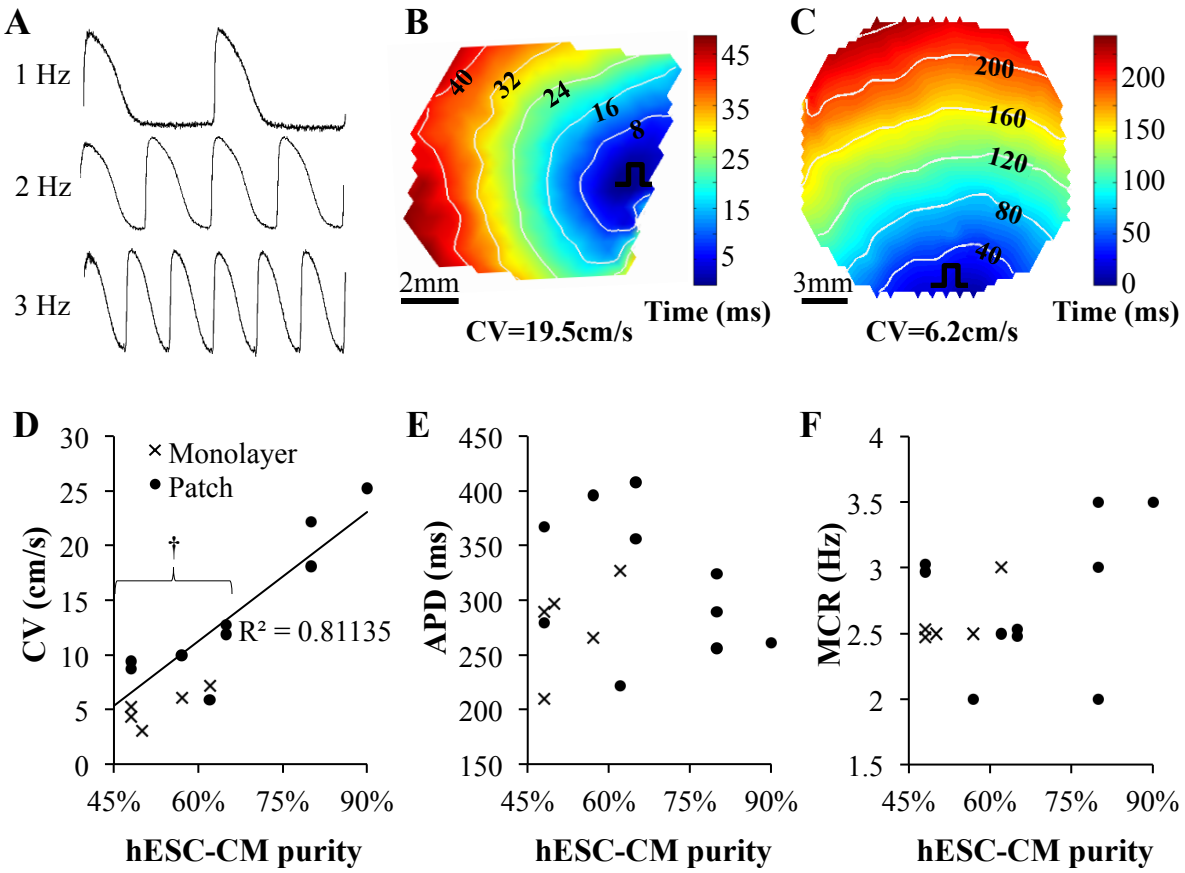

Figure 4. Action potential propagation in cardiac patches and monolayers. A) Representative optically mapped action potential traces in a 2-week old cardiac patch at various pacing rates. B,C) Representative isochrone maps during 1 Hz point stimulation of a 2-week old cardiac patch (B) and monolayer (C). D-F) Conduction velocity (D), action potential duration (E), and maximum capture rate (F) during point stimulation of cardiac patches and monolayers as a function of hESC-CM purity. †$p<0.05$ between patches and monolayers ($48\% < \text{hESC-CM purity} < 65\%$.)

Fig 5.

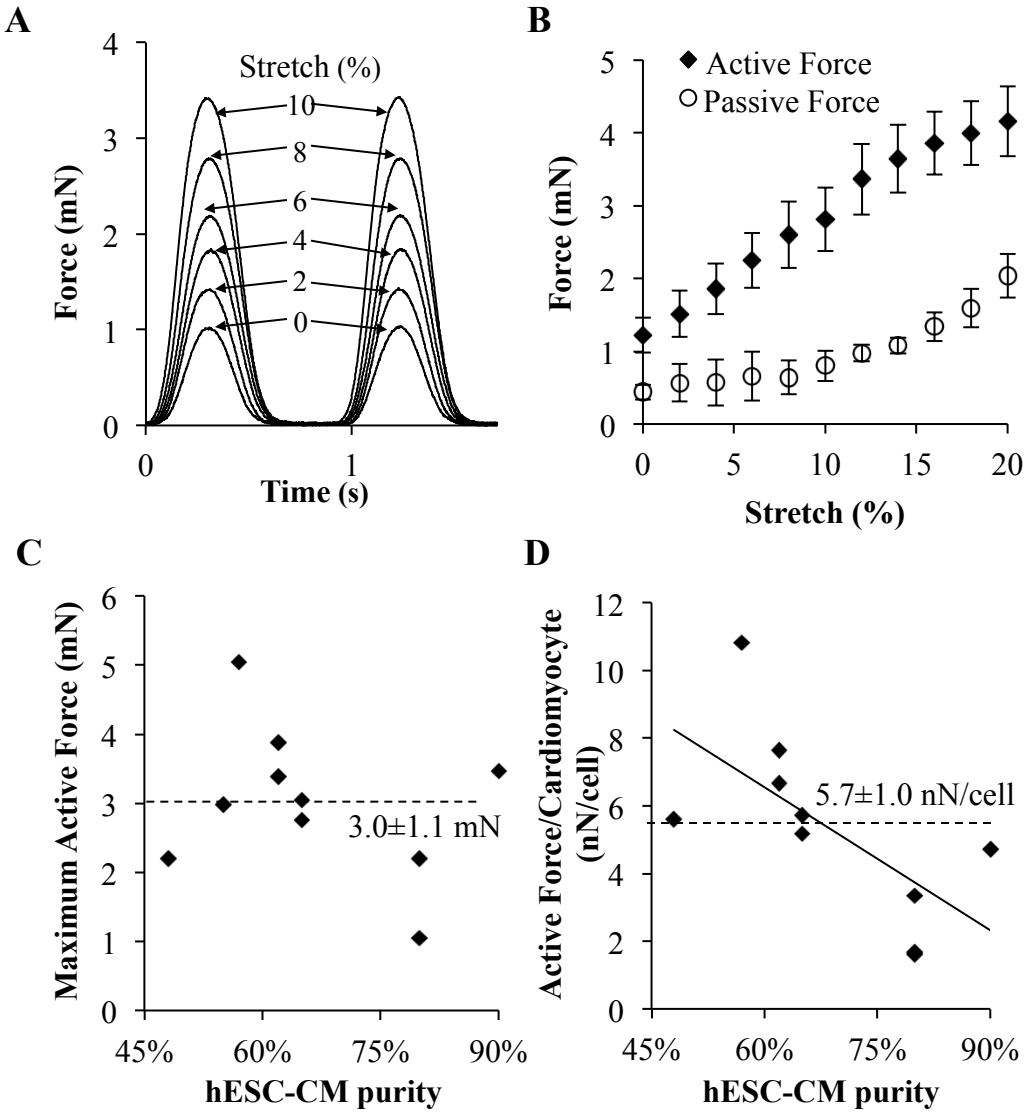

Figure 5. Contractile properties of cardiac tissue patches. A) Representative active (contractile) force traces during progressive stretch of an electrically stimulated (1Hz) 2-week cardiac patch. B) Corresponding active and passive force-length relationships in cardiac patches made with 57%-65% hESC-CMs (n=5). C) Maximum contractile force (at 1 Hz stimulation) in 2-week patches as a function of hESC-CM purity. D) Contractile force per input hESC-CM as a function of cardiomyocyte purity; $p<0.03$ for linear trend.

Fig 6.

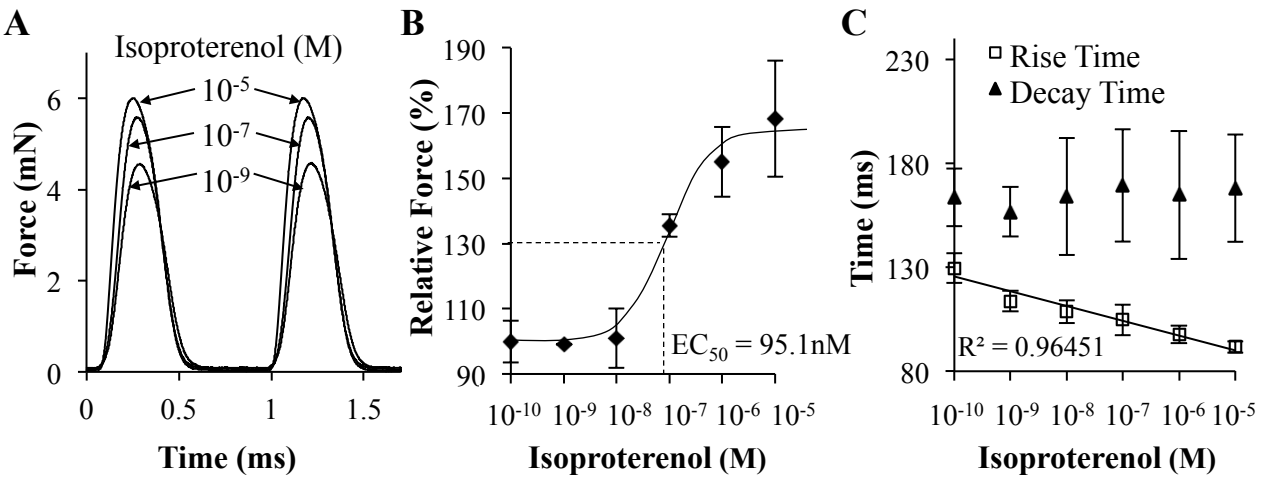

Figure 6. Inotropic response of cardiac tissue patches to beta-adrenergic stimulation. A) Representative active force traces in a tissue patch made with 55% hESC-CMs during application of increasing doses of isoproterenol (measured at 10% stretch, 1 Hz stimulation, and 0.9 mM extracellular [Ca^{2+}]). B-C) Contractile force amplitude (B) and twitch kinetics (C) as a function of isoproterenol concentration (n=4).

SUPPLEMENTAL MATERIAL

Detailed Methods

Maintenance of human embryonic stem cells

Human ES cells, trypsin-adapted HES-2, were maintained on MEF feeders in hESC medium (DMEM/F12 medium supplemented with KnockOut serum replacement (20% vol/vol, Life Technologies Corporations), L-glutamine (1mM), nonessential amino acids (0.1 mM), β-mercaptoethanol (0.1 mM), and human basic fibroblast growth factor, bFGF (20 ng/ml)).

Intracellular electrophysiological measurements

The *in vitro* effects of E-4031, terfenadine and nifedipine on action potentials recorded from hESC-CMs were measured using perforated patch whole-cell recordings with four nominal concentrations of each drug (E-4031 0.003, 0.01, 0.03, 0.1 μM; terfenadine 0.003, 0.01, 0.03, 0.1 μM; nifedipine 0.03, 0.1, 0.3, 1 μM) in at least 4-7 cardiomyocytes. Myocytes were paced continuously (stimulation rate of 1 Hz) until a stable baseline was obtained. Only cells with resting potentials more negative than –60 mV were used. Drugs were applied until steady state was achieved (5-10 min). In several instances, the application was repeated at cumulatively increased drug concentrations. All experiments were performed at physiological temperature (35±2^{o}C). Pipette solution contained in mM: 130 KCl, 5 MgCl2, 5 EGTA, 10 HEPES, pH adjusted to 7.2 with KOH and ~240 μg/mL amphotericin B to permeabilize the cell membrane. Bath solution contained in mM: 137 NaCl, 4 KCl, 1.8 CaCl2, 1 MgCl2, 10 HEPES, 10 glucose, pH adjusted to 7.4 with NaOH. After obtaining a seal (>0.8 GΩ) with a glass patch pipette, capacity current transients in voltage clamp mode were monitored for change in access resistance. An access resistance of less than 20 MΩ indicated achievement of a perforated patch recording. The patch clamp amplifier was switched to current clamp mode and a brief current pulse (up to 3 ms duration) at an appropriate level for excitation (approximately twice the voltage threshold for excitation) was used to evoke action potentials.

Cardiac monolayer culture

To compare the effect of 3D vs. 2D culture environment on hESC-CM function and maturation, we also prepared 2D cardiac monolayer cultures using cells with a range of hESC-CM purities (48-63%) similar to that used for patch fabrication. Cell suspensions were seeded on fibronectin (30 μg/ml) coated coverslips at a density of 1.3 x 10^5 cells/cm^2. Similar to cardiac patches, BrdU was added on day 0 of culture and removed after 24 h. Media was changed every 2 days thereafter.

Quantitative RT-PCR

Total RNA was extracted from cells immediately before patch and monolayer culture as well as from 4 day, 1-week and 2-week old patches and 1- and 2-week old monolayers using Qiashredder and RNeasy mini kits (Qiagen) and treated with RNase-free DNase I set according to the manufacturer's instructions. Total RNA (about 1-2 μg per 20μl reaction) was reverse transcribed using SuperScript™ II Reverse Transcriptase (Invitrogen) primed with random hexamer oligonucleotides (Promega). Quantitative PCR was carried out on CFX384 Real-Time PCR system (Bio-Rad) using Sso-Fast EvaGreen Supermix (Bio-Rad) according to the manufacturer's instructions. Relative expression levels were normalized to GAPDH and calculated using the 2−ΔCt method. All primers were purchased from Invitrogen and listed in Supplemental Table 1.

Immunofluorescence

Immunostainings were performed after 2 weeks of culture as previously described[1] using the following primary antibodies: AlexaFluor 488-conjugated mouse anti-sarcomeric α-actinin (SAA, Invitrogen A10468, Sigma A7811, 1:50 dilution), rabbit polyclonal anti-connexin43 (Cx43, Abcam A11370), mouse polyclonal anti-vimentin (Vim, Sigma A6630), rabbit polyclonal anti-von Willebrand factor (vWF, Abcam ab6994), rabbit polyclonal anti-smooth muscle 22α (SM22α, Abcam ab10135), rabbit polyclonal anti-cardiac troponin T (cTnT, Abcam, ab45932), mouse monoclonal anti-heavy chain cardiac Myosin (MHC, Abcam, ab15), and mouse monoclonal anti-N-Cadherin (N-Cad, Invitrogen 180224). Non-conjugated primary antibodies were all used at 1:200 dilutions. Secondary antibodies (Invitrogen Alexa Fluor®) were used at 1:400 dilutions. Images were taken on a Zeiss Axio Observer inverted confocal microscope and analyzed with Zeiss LSM 510 software.

Optical mapping of action potential propagation

Optical mapping of transmembrane voltage in monolayers and patches was performed using our previously described methods[1]. Briefly, cells were incubated with a voltage-sensitive dye, di4-ANEPPS (15μM, Life Technologies), in standard Tyrode's solution (in mM: 135 NaCl, 5.4 KCl, 1.8 CaCl, 1 MgCl, 0.33 NaHPO, 5 HEPES, 5 glucose), and a bipolar platinum point-electrode was used to stimulate the edge of the patch or monolayer at varying pacing rates (1-4 Hz). Blebbistatin (5 μM) was added to inhibit contractions and eliminate motion artifacts during recordings[2]. Two-second episodes of electrical activity were recorded with 0.83 ms temporal and 750 μm spatial resolution using a 504-channel photodiode array (RedShirt Imaging). Velocity of action potential propagation (conduction velocity, CV), action potential duration at 80% repolarization (APD), restitution relationships and isochrone maps and movies of action potential propagation were derived from acquired signals using our custom MATLAB software[3].

Measurements of specific contractile force and contractile force-per-input-cardiomyocyte

To derive force-length relationships, patches were progressively stretched in 2% culture length (140 μm) increments to a maximum 20% stretch (1.4 mm elongation) and passive tension was recorded in the absence of contractions. In addition, at each patch length, active (contractile) force responses were recorded during 1Hz field-electrode stimulation (10ms duration, 8-15V) applied by a Grass stimulator (SD9, Grass Technologies). Kinetic properties of contractile forces generation were determined by measuring force Rise Time (from 10% to 90% activation) and Decay Time (from 10% to 90% relaxation, Fig. S7C).

Maximum active stress (specific force) in 2-week old tissue patches was determined using our previously described methods[4]. Briefly, maximum active force that patch hESC-CMs can generate in the direction of force measurement, i.e., along long axis of elliptical pores, ($F_{max,long}$), was calculated from measured maximum active force and spatial distribution of cell alignments derived from patch F-actin images, as previously described[4, 5]. Patch porosity (P) was determined from phase contrast images of tissue patch (e.g. Fig. 1B) as the fraction of the total patch area (7x7mm^2) consisting of pores (i.e, total void area/total patch area). Average cross-sectional area (A_{av}) of the patch was calculated by multiplying patch width (7mm), average patch thickness measured from confocal stack images (e.g. Fig. S3), and patch porosity, P. Active stress (σ_{active}) was then calculated as $\sigma_{active} = \frac{F_{max,long}}{A_{av}}$.

To further quantify the efficiency of our cardiac tissue engineering method, we calculated "output force per input hES-CM" by dividing $F_{max,\,long}$, representing the functional output of our cardiac tissue-engineered system, by the number of hESC-CMs initially used for patch fabrication, representing the input into the system. This same efficiency parameter (in units of nN/cell) was also calculated for

previously reported tissue engineering methods that measured active force generation in engineered human cardiac tissues[6-9] and shown in Supplemental Table 2.

Movie legends

Supplemental Movie 1: Example of beating cardiac tissue patch after 10 days of culture.

Supplemental Movie 2: Example of optically mapped action potential propagation in a cardiac tissue patch demonstrating continuous propagation throughout the hESC-CMs.

Supplemental Movie 3: Example of optically mapped action potential propagation in a cardiac monolayer demonstrating continuous propagation throughout the hESC-CMs.

Supplemental Table S1. Primers for quantitative RT-PCR

Standard Gene name	Gene product	Forward	Reverse	size
GAPDH	GAPDH	AATGAAGGGGTCATTGATGG	AAGGTGAAGGTCGGAGTCAA	108
POU5F1	OCT4	CAAAGCAGAAACCCTCGTGC	TCTCACTCGGTTCTCGATACTG	64
NANOG	NANOG	CCCCAGCCTTTACTCTTCCTA	CCAGGTTGAATTGTTCCAGGTC	97
GATA4	GATA4	CAGGCGTTGCACAGATAGTG	CCCGACACCCCAATCTC	124
ISL1	ISL1	AAACAGGAGCTCCAGCAAAA	AGCTACAGGACAGGCCAAGA	157
MYH6	αMHC	ACCAACCTGTCCAAGTTCCG	TTGCTTGGCACCAATGTCAC	123
MYH7	ßMHC	CACAGCCATGGGAGATTCGG	CAGGCACGAAGACATCCTTCT	128
MYL2	MLC2v	GGGCGGAGTGTGGAATTCTT	CCCGGCTCTCTTCTTTGCTT	83
MYL7	MLC2a	CCAACGTGGTTCTTCCAACG	TAGGTCTCCCTCAGGTCTGC	129
TNNT2	cTNT	ATAGAGCCTGGCCTCCTTCA	CTAGGCCAGCTCCCCATTTC	130
GJA1	Cx43	TGAGCAGTCTGCCTTTCGTT	CCAGAAGCGCACATGAGAGA	94
KCNJ2	Kir2.1	TGTCACGGATGAATGCCCAA	CTGCGCCAATGATGAAAGCA	89
KCND3	Kv4.3	CACTCATCGAGAGCCAGCAT	TCTTGATGGTGGAGGTTCGT	111
SCN5A	Nav1.5	TTCAGGGCTGAAGACCATCG	GCACTTGTGCCTTAGGTTGC	142
CACNA1C	Cav1.2	ACATGCTCTTCACTGGCCTC	CCCACAACAATCAAGGCGTC	115
ATP2A2	SERCA2	TCAAGCACACTGATCCCGTC	GCTACCACCACTCCCATAGC	112
CASQ2	CASQ2	GTTGCCCGGGACAATACTGA	CTGTGACATTCACCACCCCA	142

Supplemental Table S2. Overview of electrical and mechanical properties of in vitro engineered 3D cardiac tissues

Engineered Cardiac Tissue		**Average CV** (cm/s)	**Maximum Active Force** (mN) / **Active force per iCM** (nN/cell)	**Maximum Active Stress** (mN/mm^2)	**Reference**
Scaffold Material	**Cardiogenic Cell Source**				
Collagen / Matrigel	NRVM	-	2.9	4.6	10
Collagen / Matrigel	NRVM	-	1.1	-	11
Collagen ultrafoam	NRVM	14.4	-	-	12
Collagen / Matrigel	NRVM	-	2.5	2.5*	13
Collagen / Fibrin	NRVM	-	-	0.7[a]	14
Fibrin	NRVM	23.2	1	1.1-2.1*	15
Fibrin / Matrigel	NRVM	-	~0.6	~2.1*	16
Fibrin	NRVM	-	1.3	1.8	17
Decellularized heart	NRVM	-	2.2[a]	-	18
PLGA / Fibronectin	NRVM	20.8	-	-	19
Scaffold-free bundle	NRVM	-	0.2-0.3	2-4	20, 21
Scaffold-free sheet	NRVM	2.8	-	-	22
Collagen / Matrigel	NRVM	-	0.44	0.42*	23
Collagen / Matrigel	NMVM	-	1.1[a]	1.2[a,]*	24
Collagen / Matrigel	miPSC-CM	2-3	1.4	1[a,]*	7
Collagen / Matrigel	mESC-CM	-	0.48	-	25
Collagen foam	mESC-CM	1.5	-	-	26
Fibrin / Matrigel	mESC-CM/CPC	24	2	-	1
Collagen / Matrigel	hiPSC-CM	-	0.24 / 0.7	-	6
Collagen / Matrigel	hESC-CM	< 4.9	1.4 / 1.4[b]	4.4	7
Collagen / Matrigel	hESC-CM	-	0.016* / 0.008	0.08	8
Fibrin / Matrigel	hESC-CM	-	0.061 / 0.25	0.12*	9
Fibrin / Matrigel	**hESC-CM**	**21.2**	**3.0 / 5.7**	**11.8**	**Current Study**

Native Cardiac Tissue	**Average CV**	**Maximum Active Stress**	**Reference**
Adult Rat (trabeculae)	-	40	27
Adult Rat (papillary)	-	56	28
Adult Rat (ventricle wall)	44[c]	-	13
Neonatal Rat (trabeculae)	-	9	27
Neonatal Rat (ventricle wall)	22[c]	-	29
Adult Human (ventricular strip)	-	18.3-22.8	30, 31
Adult Human (papillary muscle)	-	44	28
Adult Human (ventricle wall)	46[c]	-	32

*Estimated from cross-sectional area. [a]Estimated from figures. [b]Based on estimated 1 million hESC-CMs in 50-100 cardiac bodies. [c]Expressed as arithmetic mean of longitudinal and transverse CV. Abbreviations: NRVM, neonatal rat ventricular myocyte; NMVM, neonatal mouse ventricular myocyte; mESC-CM/CPC, mouse embryonic stem cell-derived cardiomyocyte/cardiovascular progentior; hESC-CM, human embryonic stem cell-derived cardiomyocyte; hiPSC-CM, human induced pluripotent stem cell-derived cardiomyocyte. iCM, input hESC-CM.

Supplemental References

1. Liau B, Christoforou N, Leong KW, Bursac N. Pluripotent stem cell-derived cardiac tissue patch with advanced structure and function. *Biomaterials*. 2011;32:9180-9187
2. Fedorov VV, Lozinsky IT, Sosunov EA, Anyukhovsky EP, Rosen MR, Balke CW, Efimov IR. Application of blebbistatin as an excitation-contraction uncoupler for electrophysiologic study of rat and rabbit hearts. *Heart Rhythm*. 2007;4:619-626
3. Badie N, Bursac N. Novel micropatterned cardiac cell cultures with realistic ventricular microstructure. *Biophys J*. 2009;96:3873-3885
4. Bian W, Juhas M, Pfeiler TW, Bursac N. Local tissue geometry determines contractile force generation of engineered muscle networks. *Tissue Eng Part A*. 2012;18:957-967
5. Bian W, Bursac N. Engineered skeletal muscle tissue networks with controllable architecture. *Biomaterials*. 2009;30:1401-1412
6. Streckfuss-Bömeke K, Wolf F, Azizian A, Stauske M, Tiburcy M, Wagner S, Hübscher D, Dressel R, Chen S, Jende J, Wulf G, Lorenz V, Schön MP, Maier LS, Zimmermann WH, Hasenfuss G, Guan K. Comparative study of human-induced pluripotent stem cells derived from bone marrow cells, hair keratinocytes, and skin fibroblasts. *Eur Heart J*. 2012
7. Kensah G, Roa Lara A, Dahlmann J, Zweigerdt R, Schwanke K, Hegermann J, Skvorc D, Gawol A, Azizian A, Wagner S, Maier LS, Krause A, Dräger G, Ochs M, Haverich A, Gruh I, Martin U. Murine and human pluripotent stem cell-derived cardiac bodies form contractile myocardial tissue in vitro. *Eur Heart J*. 2012
8. Tulloch NL, Muskheli V, Razumova MV, Korte FS, Regnier M, Hauch KD, Pabon L, Reinecke H, Murry CE. Growth of engineered human myocardium with mechanical loading and vascular coculture. *Circ Res*. 2011;109:47-59
9. Schaaf S, Shibamiya A, Mewe M, Eder A, Stohr A, Hirt MN, Rau T, Zimmermann WH, Conradi L, Eschenhagen T, Hansen A. Human engineered heart tissue as a versatile tool in basic research and preclinical toxicology. *PloS one*. 2011;6:e26397
10. Kensah G, Gruh I, Viering J, Schumann H, Dahlmann J, Meyer H, Skvorc D, Bar A, Akhyari P, Heisterkamp A, Haverich A, Martin U. A novel miniaturized multimodal bioreactor for continuous in situ assessment of bioartificial cardiac tissue during stimulation and maturation. *Tissue Eng Part C Methods*. 2011;17:463-473
11. Vantler M, Karikkineth BC, Naito H, Tiburcy M, Didié M, Nose M, Rosenkranz S, Zimmermann W-H. Pdgf-bb protects cardiomyocytes from apoptosis and improves contractile function of engineered heart tissue. *Journal of molecular and cellular cardiology*. 2010;48:1316-1323
12. Radisic M, Fast VG, Sharifov OF, Iyer RK, Park H, Vunjak-Novakovic G. Optical mapping of impulse propagation in engineered cardiac tissue. *Tissue Eng Part A*. 2009;15:851-860
13. Zimmermann WH, Melnychenko I, Wasmeier G, Didie M, Naito H, Nixdorff U, Hess A, Budinsky L, Brune K, Michaelis B, Dhein S, Schwoerer A, Ehmke H, Eschenhagen T. Engineered heart tissue grafts improve systolic and diastolic function in infarcted rat hearts. *Nat Med*. 2006;12:452
14. Boudou T, Legant WR, Mu AB, Borochin MA, Thavandiran N, Radisic M, Zandstra PW, Epstein JA, Margulies KB, Chen CS. A microfabricated platform to measure and manipulate the mechanics of engineered cardiac microtissues. *Tissue Engineering Part A*. 2012;18:910-919

15. Sondergaard CS, Mathews G, Wang L, Jeffreys A, Sahota A, Wood M, Ripplinger CM, Si MS. Contractile and electrophysiologic characterization of optimized self-organizing engineered heart tissue. *The Annals of thoracic surgery*. 2012;94:1241-1249
16. Hansen A, Eder A, Bonstrup M, Flato M, Mewe M, Schaaf S, Aksehirlioglu B, Schwoerer AP, Uebeler J, Eschenhagen T. Development of a drug screening platform based on engineered heart tissue. *Circ Res*. 2010;107:35-44
17. Black LD, 3rd, Meyers JD, Weinbaum JS, Shvelidze YA, Tranquillo RT. Cell-induced alignment augments twitch force in fibrin gel-based engineered myocardium via gap junction modification. *Tissue Eng Part A*. 2009;15:3099-3108
18. Ott HC, Matthiesen TS, Goh SK, Black LD, Kren SM, Netoff TI, Taylor DA. Perfusion-decellularized matrix: Using nature's platform to engineer a bioartificial heart. *Nat Med*. 2008;14:213
19. Bursac N, Loo Y, Leong K, Tung L. Novel anisotropic engineered cardiac tissues: Studies of electrical propagation. *Biochem Biophys Res Commun*. 2007;361:847-853
20. Khait L, Hodonsky CJ, Birla RK. Variable optimization for the formation of three-dimensional self-organized heart muscle. *In Vitro Cell Dev Biol Anim*. 2009;45:592-601
21. Baar K, Birla R, Boluyt MO, Borschel GH, Arruda EM, Dennis RG. Self-organization of rat cardiac cells into contractile 3-d cardiac tissue. *Faseb J*. 2005;19:275-277
22. Haraguchi Y, Shimizu T, Yamato M, Kikuchi A, Okano T. Electrical coupling of cardiomyocyte sheets occurs rapidly via functional gap junction formation. *Biomaterials*. 2006;27:4765-4774
23. Leontyev S, Schlegel F, Spath C, Schmiedel R, Nichtitz M, Boldt A, Rubsamen R, Salameh A, Kostelka M, Mohr FW, Dhein S. Transplantation of engineered heart tissue as a biological cardiac assist device for treatment of dilated cardiomyopathy. *European journal of heart failure*. 2013;15:23-35
24. de Lange WJ, Hegge LF, Grimes AC, Tong CW, Brost TM, Moss RL, Ralphe JC. Neonatal mouse–derived engineered cardiac tissue. *Circulation research*. 2011
25. Guo XM, Zhao YS, Chang HX, Wang CY, E LL, Zhang XA, Duan CM, Dong LZ, Jiang H, Li J, Song Y, Yang XJ. Creation of engineered cardiac tissue in vitro from mouse embryonic stem cells. *Circulation*. 2006;113:2229-2237
26. Song H, Yoon C, Kattman SJ, Dengler J, Masse S, Thavaratnam T, Gewarges M, Nanthakumar K, Rubart M, Keller GM, Radisic M, Zandstra PW. Interrogating functional integration between injected pluripotent stem cell-derived cells and surrogate cardiac tissue. *Proc Natl Acad Sci U S A*. 2010;107:3329-3334
27. Solaro RJ, Lee JA, Kentish JC, Allen DG. Effects of acidosis on ventricular muscle from adult and neonatal rats. *Circ Res*. 1988;63:779-787
28. Hasenfuss G, Mulieri L, Blanchard E, Holubarsch C, Leavitt B, Ittleman F, Alpert N. Energetics of isometric force development in control and volume- overload human myocardium. Comparison with animal species. *Circulation research*. 1991;68:836-846
29. Bursac N, Papadaki M, Cohen RJ, Schoen FJ, Eisenberg SR, Carrier R, Vunjak-Novakovic G, Freed LE. Cardiac muscle tissue engineering: Toward an in vitro model for electrophysiological studies. *American Journal of Physiology - Heart and Circulatory Physiology*. 1999;277:H433-H444
30. Mulieri LA, Hasenfuss G, Leavitt B, Allen PD, Alpert NR. Altered myocardial force-frequency relation in human heart failure. *Circulation*. 1992;85:1743-1750

31. Holubarsch C, Ludemann J, Wiessner S, Ruf T, Schulte-Baukloh H, Schmidt-Schweda S, Pieske B, Posival H, Just H. Shortening versus isometric contractions in isolated human failing and non-failing left ventricular myocardium: Dependency of external work and force on muscle length, heart rate and inotropic stimulation. *Cardiovascular research*. 1998;37:46-57
32. Durrer D, van Dam RT, Freud GE, Janse MJ, Meijler FL, Arzbaecher RC. Total excitation of the isolated human heart. *Circulation*. 1970;41:899-912

Supplemental Fig S1.

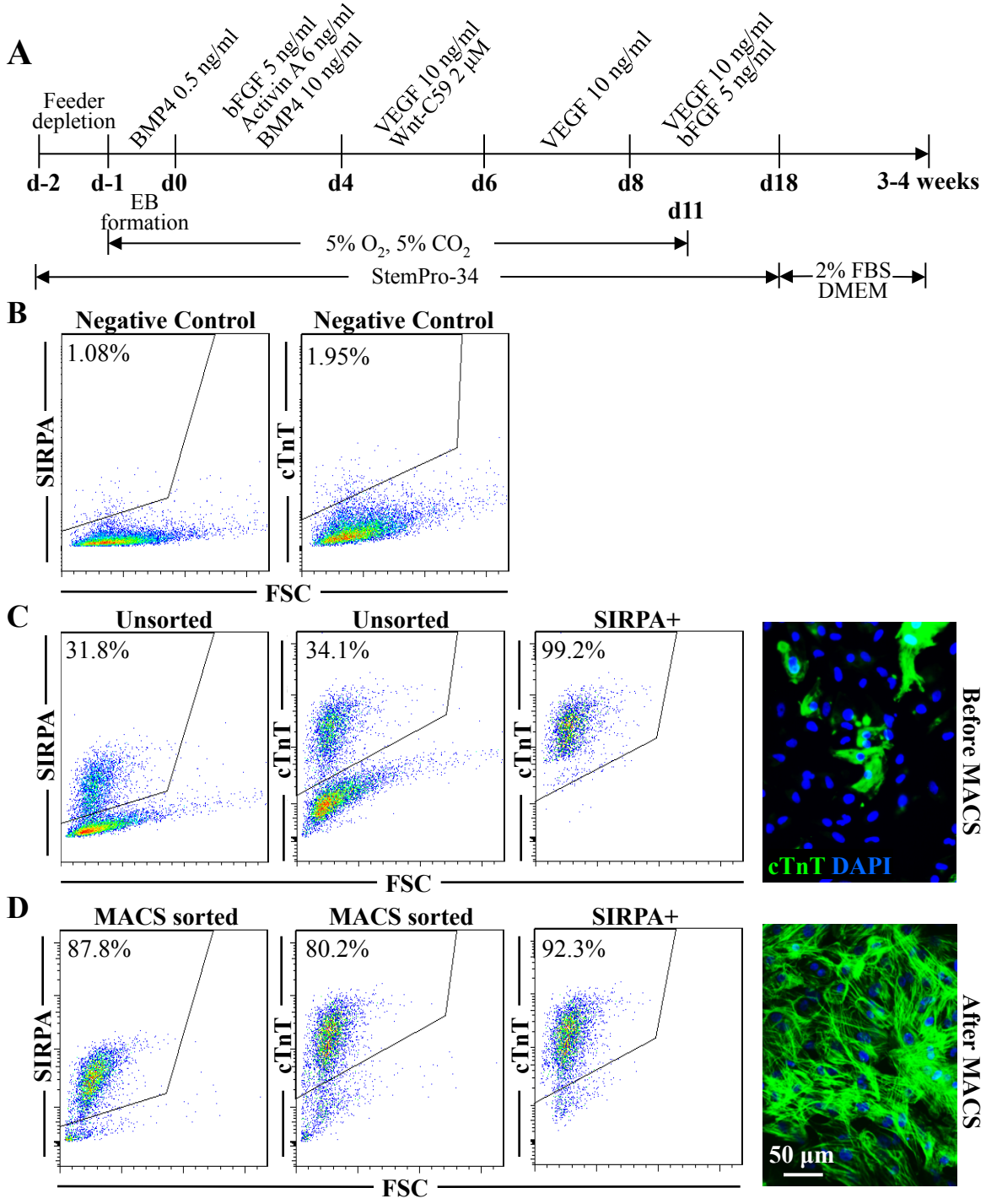

Supplemental Fig S1. Flow cytometry analysis of hESC-CM purity before and after MACS purification using SIRPA antibody. A) hESC cardiac differentiation protocol. After 3-4 weeks of differentiation, cells were purified/analyzed by MACS/FACS and used for patch and monolayer culture. B) Negative control PE and FITC isotypes. C) Pre-MACS flow cytometry analysis of SIRPA-PE (left), cTnT-FITC (middle), and cTnT in SIRPA gate (right). Immunostaining before MACS purification shows sparse $cTnT^+$ cells. D) Post-MACS flow cytometry analysis of SIRPA-PE (left), cTnT-FITC (middle), and cTnT in SIRPA gate (right). Immunostaining after MACS purification shows abundant $cTnT^+$ cells. Note that in unsorted and MACS purified cells, 92-99% of $SIRPA^+$ cells are also $cTnT^+$. FSC, Forward-scattered light. cTnT, cardiac troponin T.

Supplemental Fig S2.

A

Control	APD_{30} (ms)	APD_{60} (ms)	APD_{90} (ms)	RMP (mV)	APA (mV)	$(dV/dt)_{max}$ (V/s)
Mean ± SEM (n= 79)	159.4 ± 7.1	195.5 ± 8.5	221.3 ± 8.8	-70.9 ± 0.5	102.9 ± 1.0	38.1 ± 1.5

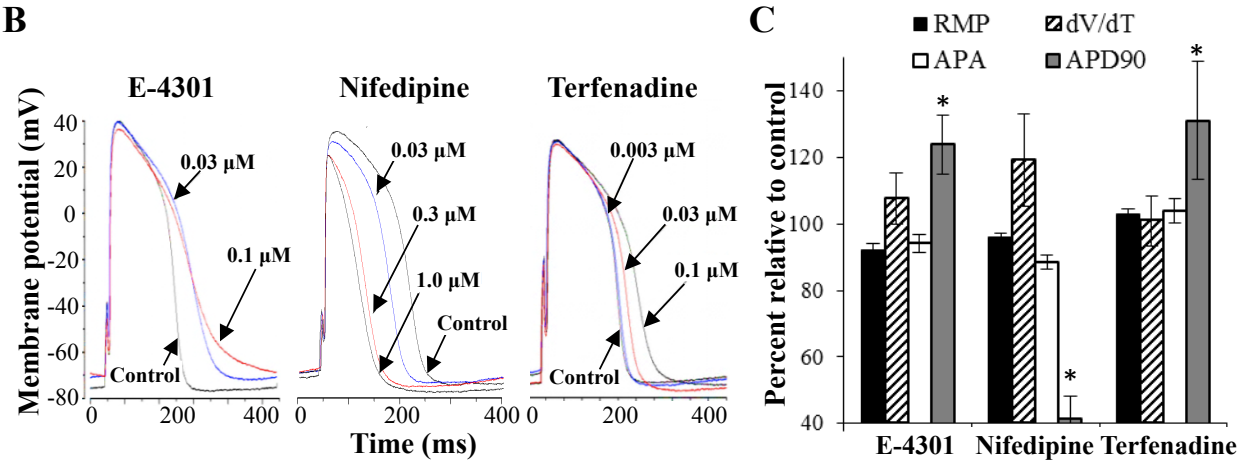

Supplemental Fig S2. Electrophysiological characteristics of hESC-CMs. A) Action potential (AP) properties of drug-free (control) hESC-CMs. B) Whole cell current-clamp traces of membrane voltage in hESC-CMs in the presence of different concentrations of HERG K^+ channel blocker E-4031 (left), L-type Ca^{2+} channel blocker nifedipine (middle), and ATP-sensitive K^+ channel blocker terfenadine (right). C) Quantification of resting membrane potential (RMP), AP upstroke velocity (dV/dt_{max}), AP amplitude (APA), and AP duration at 90% repolarization (APD90) in hESC-CMs treated with either E-4031 (0.1uM, n=7), nifedipine (1µM, n=6), or terfenadine (0.1uM, n=4) relative to vehicle control (100%); *p<0.05 compared with control.

Supplemental Fig S3.

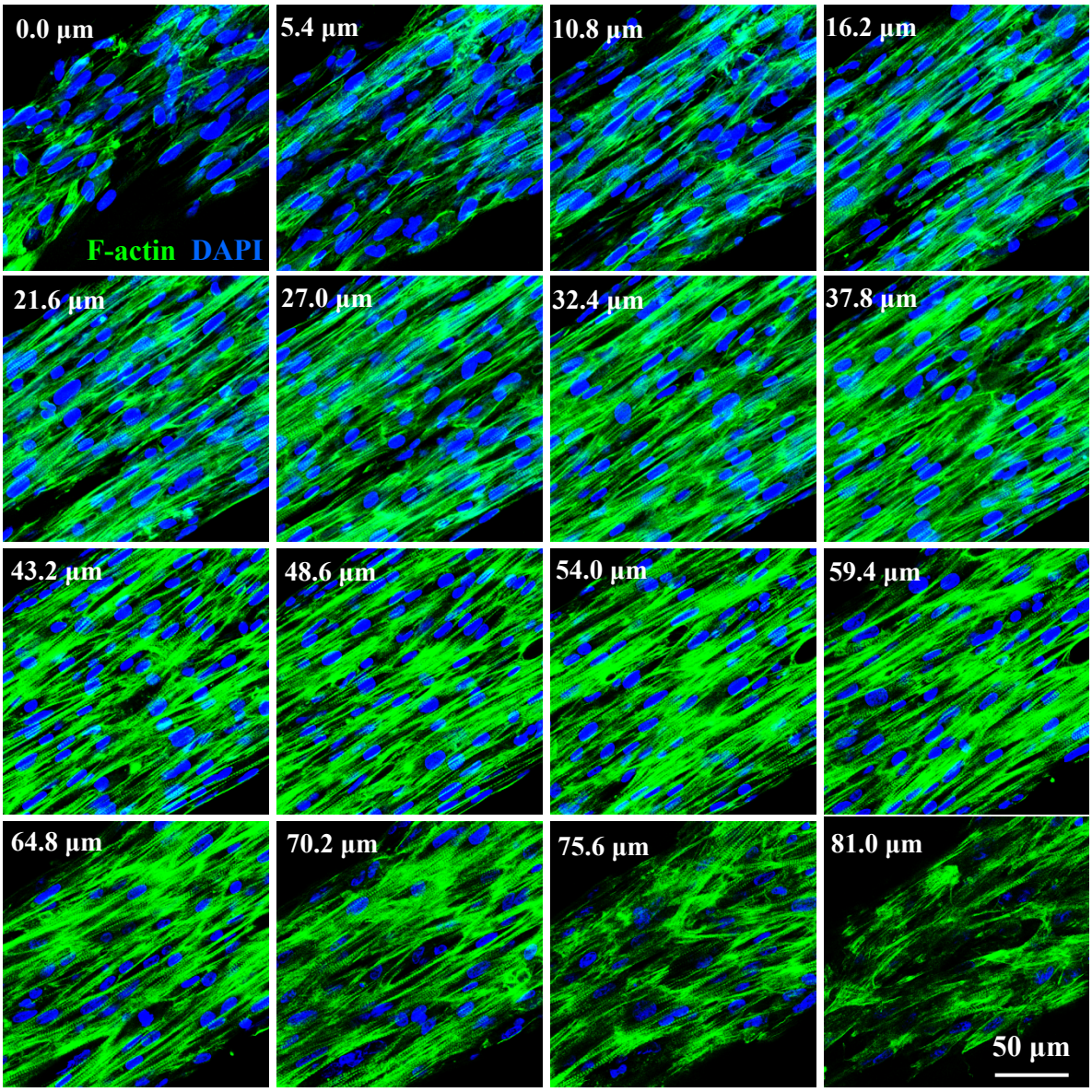

Supplemental Fig S3. Representative confocal image stack demonstrating uniform hESC-CM density and alignment throughout the thickness of a 2-week old cardiac tissue patch. Numbers in the top left corner denote imaging depth inside the patch. Green, F-actin; blue, DAPI. The patch was made of differentiated hESCs containing 70% hESC-CMs.

Supplemental Fig S4.

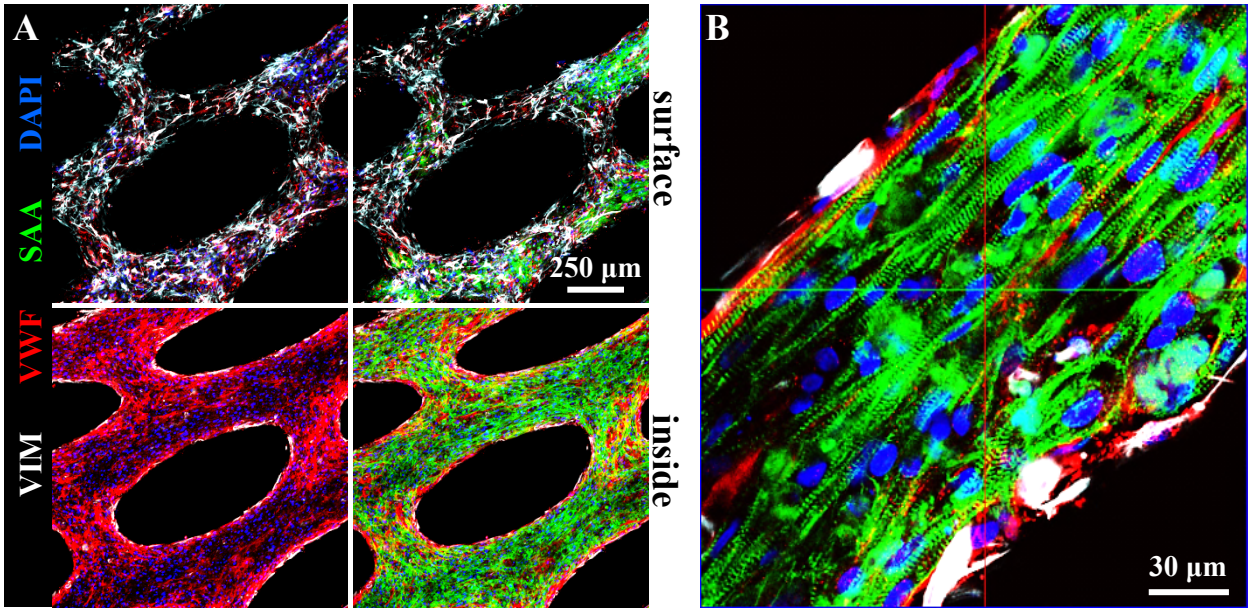

Supplemental Fig S4. Cellular composition of cardiac tissue patches. A) Representative immunostaining of a tissue patch made with 65% hESC-CMs showing that endothelial cells double-positive for von Willebrand factor (vWF) and Vimentin (Vim) were interspersed throughout the patch while Vim^{+}/vWF^{-} cells (fibroblasts) were mainly present on the patch surface. B) Sarcomeric alpha actinin (SAA)-positive cross-striated cardiomyocytes were aligned throughout the patch (also shown in top-right and bottom-right panels in A).

Supplemental Fig S5.

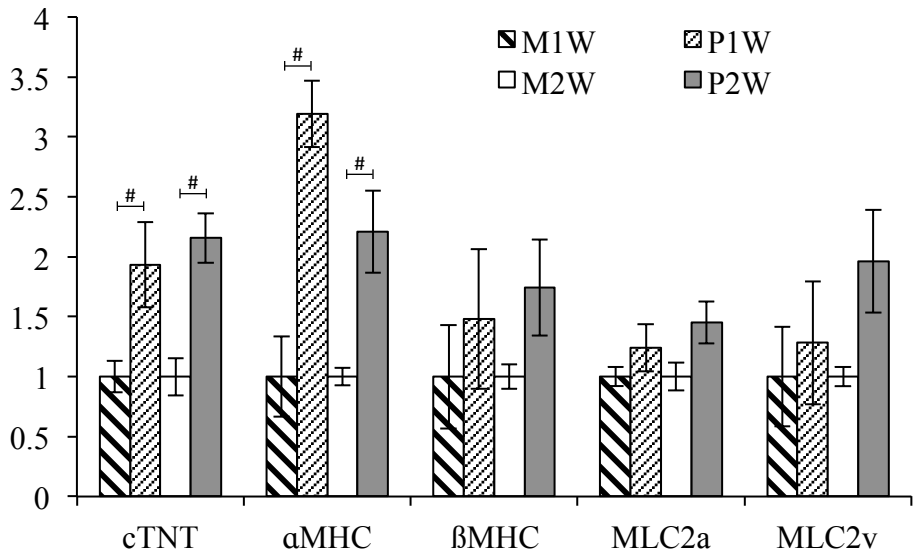

Supplemental Fig S5. Comparative expression of genes important for cardiac contractile function in age-matched 2D monolayers and 3D tissue patches. M1W and MW2, 1- and 2-week old monolayers; P1W and P2W, 1- and 2-week old tissue patches. cTnT, Cardiac troponin T; αMHC, alpha-myosin heavy chain; βMHC, beta-myosin heavy chain; MLC2a, myosin light chain-2 atrial; MLC2v, myosin light chain-2 ventricular. Gene expression levels in patches are shown normalized to those of age-matched monolayers. #, significant difference between patches and monolayers (n = 2-4, with 3 technical replicates). Monolayers and patches were made from differentiated hESCs containing 60-65% hESC-CMs.

Supplemental Fig S6.

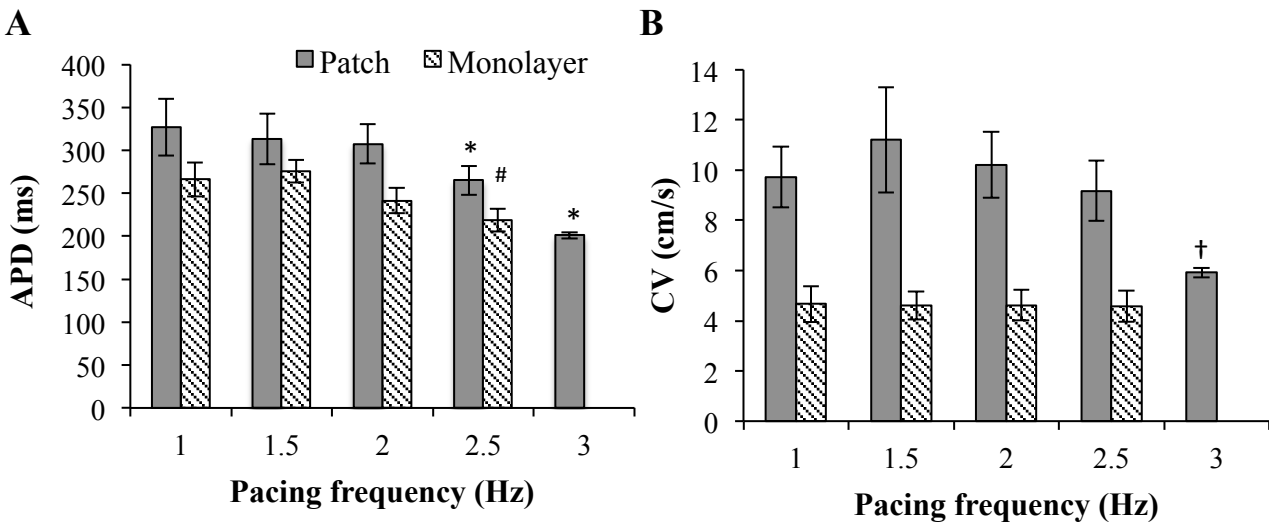

Supplemental Fig S6. Electrical restitution relationships in 2-week old cardiac tissue patches and monolayers. A-B) Dependence of action potential duration (APD) and conduction velocity (CV) on pacing frequency. *$p<0.05$ relative to all other pacing rates. #$p<0.05$ relative to 1.5 and 2 Hz pacing rates; †$p<0.05$ relative to 1, 1.5, and 2Hz pacing rates. n = 4-5 monolayers, 5 patches between 1-2.5Hz) and 2 patches at 3Hz. Monolayers and patches were made from differentiated hESCs containing 48-65% hESC-CMs.

Supplemental Fig S7.

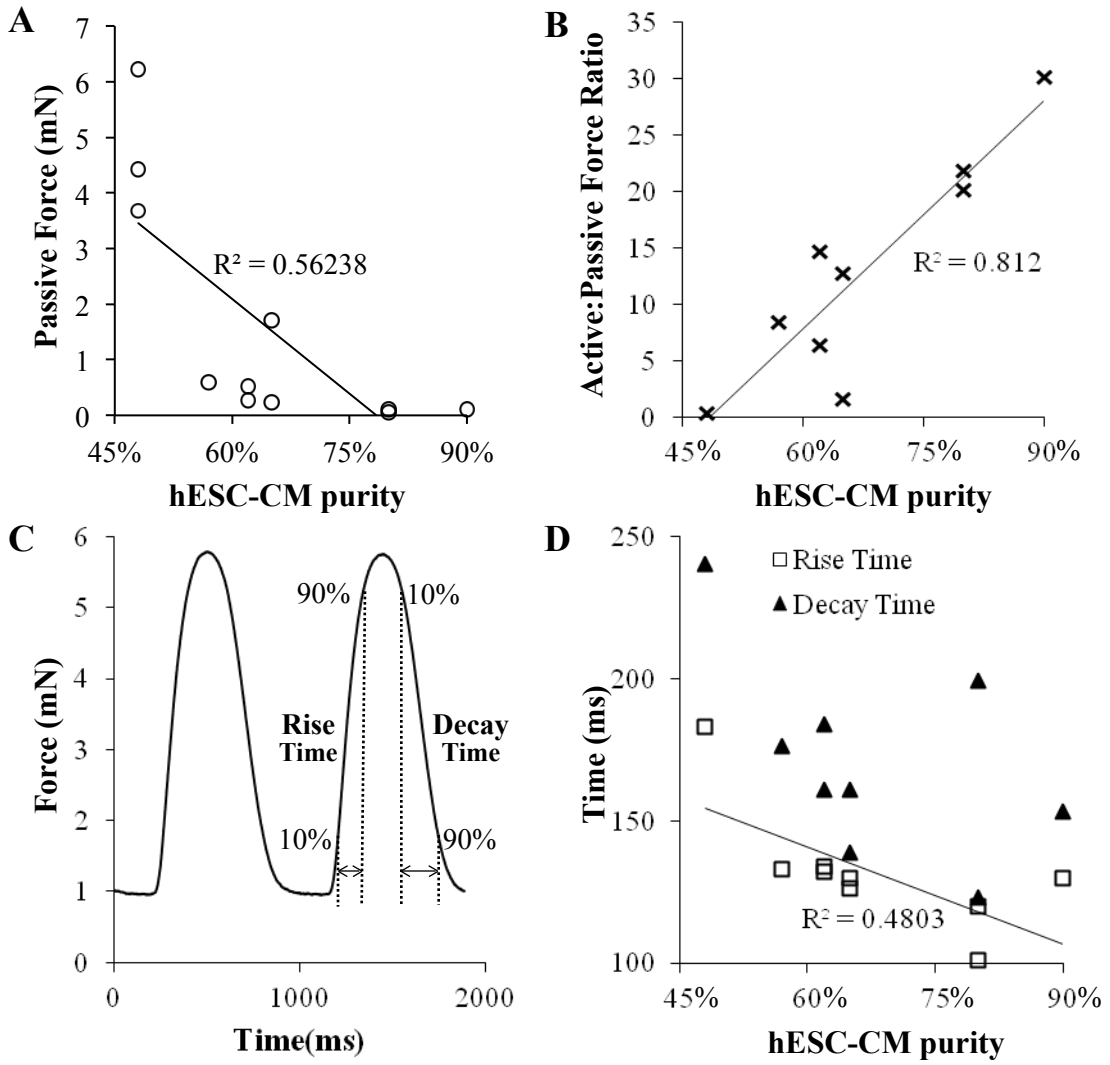

Supplemental Fig S7. Contractile properties of 2-week old cardiac tissue patches. A) Passive tension of tissue patches decreases with increased hESC-CM purity of cells used for patch production. B) Active:passive force ratio increases linearly with hESC-CM purity. Forces in A-B are measured at 10% stretch during 1Hz stimulation. C) Representative isometric twitch force traces in cardiac tissue patches (measured at 10% stretch and 1Hz stimulation. D) Rise and Decay Times of twitch traces (measured as shown in C) as a function of hESC-CM purity. While both Rise and Decay Times appear to decrease with increase in cardiomyocyte purity, only the Rise Time shows statistically significant trend (R^2=0.48, $p<0.02$).